

1 **Small emission sources in aggregate disproportionately account**
2 **for a large majority of total methane emissions from the US oil**
3 **and gas sector**

4 James P. Williams¹, Mark Omara^{1,2}, Anthony Himmelberger², Daniel Zavala-Araiza¹, Katlyn
5 MacKay¹, Joshua Benmergui^{1,2,3}, Maryann Sargent³, Steven C. Wofsy³, Steven P. Hamburg^{1,2},
6 Ritesh Gautam^{1,2}

7 ¹Environmental Defense Fund, New York, NY, USA 10010

8 ²MethaneSAT, LLC, Austin, TX, USA 78701

9 ³Harvard University, Cambridge, MA, USA 02138

10
11 *Correspondence to:* James P. Williams (jamwilliams@edf.org), Ritesh Gautam (rgautam@edf.org)
12

13
14 **Abstract.** Reducing methane emissions from the oil and gas (oil/gas) sector has been identified as a critically
15 important global strategy for reducing near-term climate warming. Recent measurements, especially by satellite and
16 aerial remote sensing, underscore the importance of targeting the small number of facilities emitting methane at high
17 rates (i.e., “super-emitters”) for measurement and mitigation. However, the contributions from individual oil/gas
18 facilities emitting at low emission rates that are often undetected are poorly understood, especially in the context of
19 total national- and regional-level estimates. In this work, we compile empirical measurements gathered using
20 methods with low limits of detection to develop facility-level estimates of total methane emissions from the
21 continental United States (CONUS) midstream and upstream oil/gas sector for 2021. We find that 70% (95%
22 confidence intervals: 61-81%) of the total 14.6 (12.7-16.8) Tg/yr oil/gas methane emissions in the CONUS for the
23 year 2021 originate from facilities emitting <100 kg/hr, and 30% (26-34%) and ~80% (68-90%) from facilities
24 emitting <10 kg/hr and <200 kg/hr, respectively. While there is variability among the emission distribution curves
25 for different oil/gas production basins, facilities with low emissions are consistently found to account for the
26 majority of total basin emissions (i.e., range of 60% - 86% of total basin emissions from facilities emitting <100
27 kg/hr). We estimate that production well sites were responsible for 70% of regional oil/gas methane emissions, from
28 which we find the well sites that accounted for only 10% of national oil and gas production in 2021,
29 disproportionately accounted for ~~77%~~ ~~(7267-9081%)~~ of the total well site emissions. Our results are also in broad
30 agreement with data obtained from several independent aerial remote sensing campaigns (e.g., MethaneAIR, Bridger
31 Gas Mapping LiDAR, AVIRIS-NG, and Global Airborne Observatory) across 5-8 major oil/gas basins. Our findings
32 highlight the importance of accounting for the significant contribution of small emission sources to total oil/gas
33 methane emissions. While reducing emissions from high-emitting facilities is important, it is not sufficient for the
34 overall mitigation of methane emissions from the oil and gas sector which according to this study is dominated by
35 small emission sources across the US. Tracking changes in emissions over time and designing effective mitigation
36 policies should consider the large contribution of small methane sources to total emissions.

37

39 1 Introduction

40

41 Methane is a short-lived but powerful greenhouse gas with a global warming potential more than 80 times
42 stronger than carbon dioxide (CO₂) over 20 years (AR6 Synthesis Report: Climate Change 2023, 2024). Therefore,
43 the reduction of methane emissions has become a key goal to achieve rapid climate mitigation in the short term
44 (Ocko et al., 2021). In North America, one of the largest sources of methane emissions originates from the oil and
45 gas (oil/gas) sector, with most emissions originating from the production (i.e., upstream) and transportation/storage
46 (i.e., midstream) sectors (Alvarez et al., 2018). Multiple studies, especially over the past decade, have focused on the
47 quantification of methane sources from the oil/gas sector, with particular emphasis on the continental United States
48 (CONUS) (Alvarez et al., 2018; de Gouw et al., 2020; Omara et al., 2018; Lu et al., 2022; Zhang et al., 2020; Shen
49 et al., 2022; Cusworth et al., 2022; Nesser et al., 2023; Brandt et al., 2016; Duren et al., 2019; Maasackers et al.,
50 2021; Lu et al., 2023; Worden et al., 2022). Several studies have recognized the importance of a small percentage of
51 high-emitting sites (i.e. “super-emitters”) and reported them as accounting for a large fraction of total methane
52 emissions (Brandt et al., 2016; Cusworth et al., 2022; Duren et al., 2019; Sherwin et al., 2024). The emission rate
53 thresholds that characterize these super-emitting facilities are critical information for methane measurement
54 platforms, especially remote sensing technologies focused on detecting high-emitting point sources. Aerial and
55 satellite remote sensing technologies have enabled more frequent monitoring of emissions from oil and gas sites and
56 rapid mapping of large areas, although they face limitations in detection sensitivity. Despite the improved ability to
57 locate and quantify emissions from high-emitting sites, there has been considerable lack of understanding about the
58 characteristics of low methane emitting facilities, especially those emitting at rates below the limits of detection
59 (LOD) of most point-source detection remote sensing platforms, and their contributions to total oil/gas methane
60 emissions.

61 While some studies offer important yet limited insights into the contributions of different lower-emitting
62 infrastructure from the CONUS oil/gas sector, there is a lack of understanding about their overall contribution to the
63 total sectoral regional and national scale emissions. A recent study by Xia et al. (2024) combined aerial remote
64 sensing data from Bridger Gas Mapping LiDAR (Bridger GML) in four oil/gas basins supplemented with
65 component-level modeling for facilities emitting below the Bridger GML LOD and found significantly more
66 emission sources in the 1 – 10 kg/hr range when compared to the emission distribution used by the EPA (Xia et al.,
67 2024). In a study focused on production well sites in the CONUS, the main source of methane emissions from the
68 oil/gas sector (Alvarez et al., 2018; Omara et al., 2018; Rutherford et al., 2021), Omara et al. (2018) found that 90%
69 of total methane emissions from producing well sites came from those emitting at rates <100 kg/hr. A follow-up
70 study by Omara et al. (2022) highlights that the total methane emissions from low-producing well sites producing
71 less than 15 boe/day (i.e., 1 Mcf = 1,000 cubic feet of natural gas = 19.2 kg of methane at 15.6 °C and 1 atmosphere;
72 1 boe = 1 barrel of oil equivalent = 6 Mcf; assumed methane content in natural gas of 80%), which comprise 80% of

73 all producing well sites in the CONUS, were responsible for nearly half of all methane emissions from the oil/gas
74 production sector. Kunkel et al. (2023) observed that the use of the Bridger GML remote sensing platform with an
75 LOD of 3 kg/hr, combined with prior Carbon Mapper detections in a section of the Permian basin showed a
76 significant contribution from sources below the listed LOD of Carbon Mapper of 10 kg/hr. Cusworth et al. (2022)
77 found that 35% of total methane emissions (including non-oil/gas sources) from several major oil/gas producing
78 basins (other than the Appalachian basin) in the CONUS come from facilities emitting >10 kg/hr, indicating that
79 65% of emissions come from facilities emitting <10 kg/hr. Although these studies using independent measurement
80 platforms provide new emerging insights about the importance of low methane emitting oil/gas facilities, there
81 generally remains a lack of quantitative assessment of the relative fractions of emissions originating from different
82 emission rate thresholds aggregated over individual oil/gas basins as well as at a national scale.

83 There are a variety of different methane quantification methods that differ in terms of their spatial resolution of
84 sources, logistical constraints, costs of implementation, and their LODs. Measurement method sensitivities and
85 LODs have important policy implications. For example, the Environmental Protection Agency (EPA) recently
86 finalized regulations that define a “super-emitter event” as an emission rate threshold of 100 kg/hr or greater
87 (Standards of Performance for New, Reconstructed, and Modified Sources and Emissions Guidelines for Existing
88 Sources: Oil and Natural Gas Sector Climate Review, 2024), albeit without clear information on what percentage of
89 total regional emissions are captured within this definition. Satellite and aerial remote sensing methods have point
90 source LODs that range anywhere from 1-3 kg/hr for Bridger’s airborne GML (Johnson et al., 2021; Kunkel et al.,
91 2023; Thorpe et al., 2024; Xia et al., 2024) to ~200 kg/hr for GHGSat (Sherwin et al., 2023). In contrast, ground-
92 based measurement methods such as OTM-33a and tracer release have LODs <1 kg/hr (Fox et al., 2019). A study by
93 Ravikumar et al. (2018) using the Fugitive Emissions Abatement Simulation Toolkit (FEAST) suggests that a
94 method with a LOD of 0.1-1 kg/hr would sufficiently capture all emissions from the oil/gas sector, whereas the
95 ability to quantify emissions below this threshold would not lead to any significant increases in mitigation.
96 Ultimately, there is a need for clarification in the total percentage contribution of emissions originating from a given
97 emission rate threshold, which requires characterizing entire emissions distributions, not only the high emitters.

98 In this work, we create and analyze measurement-based methane emission rate distributions of US upstream and
99 midstream oil/gas facilities to determine the percentage contributions of different emission rate thresholds to total
100 methane emissions. First, we use empirical measurements gathered from ground-based sampling platforms to
101 develop a bottom-up facility-based model to estimate methane emissions for upstream and midstream facilities in
102 the continental US (CONUS) for 2021. Next, we aggregate our facility-level, population-based data to determine the
103 national- and basin-level contributions of methane emissions originating from facilities emitting at different
104 emission rate thresholds, in addition to comparisons to aerial-remote sensing platforms. Finally, we break down the
105 emission distribution curves by facility category to analyze how the percentage contributions of total emissions vary
106 across facility types.

107

108 **2 Materials and methods**

109

110 **2.1 Empirical measurements**

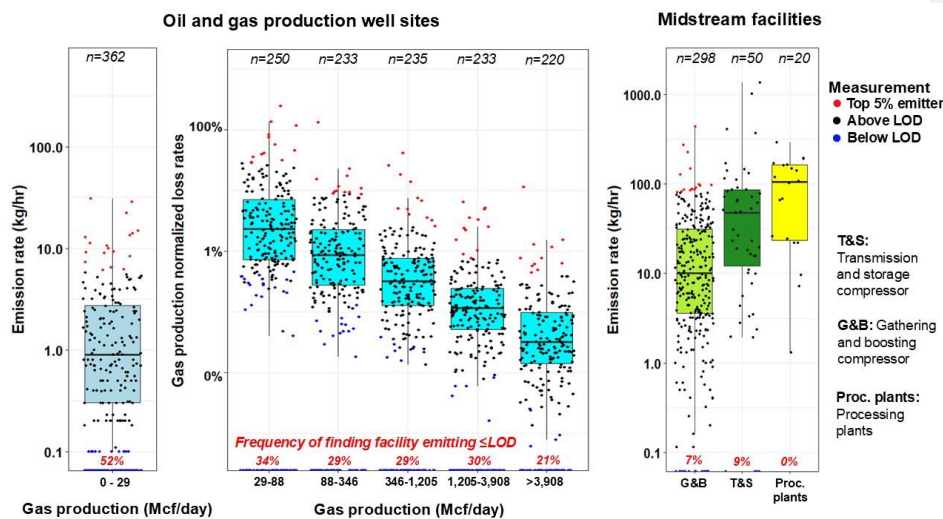
111

112 We compile 1,901 facility-level methane emission rate measurements from 16 studies (Brantley et al., 2014;
113 Caulton et al., 2019; Deighton et al., 2020; Goetz et al., 2015; Lan et al., 2015; Mitchell et al., 2015; Omara et al.,
114 2016, 2018; Rella et al., 2015; Riddick et al., 2019; Robertson et al., 2017, 2020; Subramanian et al., 2015;
115 Yacovitch et al., 2015; Zhou et al., 2021; Zimmerle et al., 2020) that use ground-based site/facility level and
116 source/component level measurement methods with low LOD's of ~0.1 kg/hr. Most (i.e., 85%) of empirical
117 measurements we use in this work were gathered using ground-based mobile laboratories that quantified methane
118 emissions at the site/facility level using either tracer-based releases, the EPA Other Test Method (OTM-33a), or
119 Gaussian plume transport modeling (Fox et al., 2019) (Table S2). The remaining 15% of empirical measurements we
120 use (Deighton et al., 2020; Riddick et al., 2019; Zimmerle et al., 2020) are ground-based methods that aggregated
121 source/component-level HiFlow sampling or static/dynamic chamber measurements, which could mean that other
122 on-site emission sources were not quantified during measurement and overall emission rate estimates are
123 conservative. [Only one study was excluded from our analysis](#) (ERG, 2011) [due to a combination of age and a focus](#)
124 [on component-level measurements](#).

125 The compiled empirical measurements target a variety of production well sites and/or midstream facilities
126 across at least nine oil/gas-producing basins in the CONUS (Table S3). For all facility categories (i.e., production
127 well sites, gathering and boosting compressor stations, transmission and storage compressor stations, and processing
128 plants), we prioritize datasets of randomly sampled sites that include measurements below the method's LOD or
129 reported as zero emissions, except for measurements from two studies (Brantley et al., 2014; Lan et al., 2015) which
130 we discuss later in Section 2.3. Additionally, for production well site measurements, we focus only on data that
131 provide facility-level gas production data for the date/month of measurement. Our compiled dataset of
132 measurements includes both routine intentional (e.g., venting from pneumatic devices) and non-intentional (e.g.,
133 malfunctioning equipment and/or leaks from valves, connectors, flanges, etc) emissions, and while we remove any
134 measurements attributed to high emitting intermittent events such as flowbacks and liquids unloadings if that
135 information is present, we cannot fully discount that emissions from these high-emitting intermittent sources are
136 included in our compiled dataset. Furthermore, we remove any empirical measurement data associated with flaring
137 emissions, which are treated separately as discussed below, if that information is provided in the empirical data.

138 We categorize the empirical measurements by facility category as production well sites, gathering and boosting
139 compressor stations (G&B compressors), transmission and storage compressor stations (T&S compressors), or
140 processing plants. We group the empirical measurements from production well sites into six production bins based
141 on gross average daily gas production as reported in individual studies. We use gross daily average gas production
142 data instead of oil and gas production data for two reasons: 1) the limited availability of facility-level oil production
143 data provided from empirical measurement studies; and 2) the established relationship between gas production and

144 emission rates observed in previous work (Omara et al., 2018, 2022, 2024). The gas production ranges of the
 145 production bins (Fig. 1) are chosen to evenly distribute empirical measurements above the method LOD to all six
 146 production bins. This categorization creates nine distinct facility categories: G&B compressors, T&S compressors,
 147 processing plants, and six groups of production well sites. We further classify the nine distinct facility categories
 148 into five primary facility categories: low-production well sites which produce combined oil and gas <15 boe/day
 149 (i.e., 0.13 kt of methane production per year), non-low-producing well sites which produce ≥ 15 boe/day, processing
 150 plants, G&B compressors, and T&S compressors. In addition to these facility categorizations, we also include
 151 Visible Infrared Imaging Radiometer Suite (VIIRS) flare detections and flared gas volume estimates in our analysis,
 152 which are treated as an independent methane source since flares can be located on multiple facility categories across
 153 the upstream and midstream oil/gas sectors.



154
 155 **Figure 1:** Facility-level empirical measurement data distributed by different distinct facility categories for production well sites
 156 (left) and midstream facilities (right). Individual measurements are shown for each box plot and colored according to their
 157 emission rate status for that facility category, where blue points are considered non-detectable emissions below an emission rate
 158 threshold of ≤ 0.1 kg/hr/facility which is the method LOD we use, black points are measurements above our method LOD but
 159 below the top 5% emitter category, and red points are the top 5% of empirical emission rates or loss rates for that facility
 160 category. The number of empirical measurements available for each facility category is denoted at the top of each boxplot. The
 161 estimated mean frequency of finding a facility emitting below the method LOD is shown in inset red text at the bottom of each
 162 boxplot. We show absolute emission rates (kg/hr) rather than normalized loss rates (%) for the lowest cohort of production well
 163 sites due to the reasoning presented in Section 2.3. Unit conversions: 1 Mcf = 1,000 cubic feet of natural gas = 19.2 kg of
 164 methane at 15.6 °C and 1 atmosphere; 1 boe = 1 barrel of oil equivalent = 6 Mcf; assumed methane content in natural gas of 80%.

165
 166 **2.2 Activity data**
 167

168 We use activity data (i.e., number of facilities and spatial locations) for actively producing wells in 2021
169 provided by Enverus for the CONUS. We calculate both the annual averaged daily gross gas production, and oil and
170 gas production for each producing well using the number of producing days and total annual oil and gas production
171 data provided by Enverus. We convert production wells to production well sites by spatially aggregating individual
172 wells within 25-meter (vertical wells) or 50-meter (horizontal wells) distances from each other and separately
173 merging their combined oil and gas production and gas production, and converting these production values to a mass
174 equivalent production rate in kg/hr of methane (i.e., 1 Mcf = 1,000 cubic feet of natural gas = 19.2 kg of methane at
175 15.6 °C and 1 atmosphere; 1 boe = 1 barrel of oil equivalent = 6 Mcf; assumed methane content in natural gas of
176 80%), similar to previous approaches (Omara et al., 2018).

177 We acquire activity data for operational transmission and storage (T&S) and gathering and boosting (G&B)
178 compressor stations and processing plants from Enverus for 2021 for the CONUS, which was further supplemented
179 by additional data from the Oil and Gas Infrastructure Mapping (OGIM) database published in Omara et al. (2023).
180 We filter data for these midstream facilities to include only active facilities in the year 2021. For VIIRS flare
181 detections, we use the 2021 natural gas flared volume estimates based on natural gas flaring detections provided by
182 the VIIRS instruments installed aboard satellite platforms which have a 750x750 meter source resolution (NOAA-20
183 and Suomi National Polar-orbiting Partnership) (Elvidge et al., 2015). In terms of potential double-counting between
184 the VIIRS flare detections and the empirical measurements we use in this work, the majority of VIIRS detections are
185 in the Permian, Bakken, and Eagle Ford oil/gas basins (i.e., 86% of total VIIRS detections) which corresponds to a
186 small number of our empirical measurement data (Table S3) (Plant et al., 2022). However, the limited availability of
187 spatial coordinates for our empirical measurements restricts our ability to perform a direct comparison to exclude
188 overlapping/proximal VIIRS detections and our facility-level empirical measurements. Therefore, we do
189 acknowledge that there is a possibility of double counting between our empirical measurement data and the VIIRS
190 flare detections, but we expect the degree of overlap to be low.

191 **2.3 Facility-level methane emission inventory**

192 We calculate annual methane emissions from all facility categories (i.e., six production bins of production well
193 sites, T&S compressor stations, G&B compressor stations, processing plants, and VIIRS flare detections) using a
194 multi-step probabilistic modeling approach adapted from multiple studies (Omara et al., 2018, 2022; Plant et al.,
195 2022) (Fig. 2). Briefly, for each individual facility and VIIRS flare detection in the CONUS for 2021, we estimate an
196 annually averaged methane emission rate using empirical measurement data, and consequently the cumulative
197 distribution of methane emission rates from the aggregation of these individual emission rates. Each emission rate
198 estimate is indexed according to the corresponding replicate (n=500), and we use these repetitions to determine
199 uncertainty for the cumulative methane emission distribution curves. The detailed steps of this process for all facility
200 categories and VIIRS flare detections are described below.

201 For the highest five gas production bins of producing well sites ranging from 29 to >3,908 Mcf/day (or 0.2 to
202 >27 kt of methane production per year, Figure 1), we use gross gas production normalized loss rates to model the

203 distributions used to calculate methane emission rates from Eq. (1), where the: *Loss rate* is the fraction of emitted
204 gas relative to gas production, the *emission rate* is rate of methane emitted from a facility in kilograms per hour,
205 σ_{CH_4} is the methane content of the emitted gas which we assume to be 80%, and the *gas production* is the mass
206 equivalent of natural gas produced in kilograms per hour at 1 atmosphere and 15.6 °C (1 Mcf = 1,000 cubic feet of
207 natural gas = 19.2 kg of methane at 15.6 °C and 1 atmosphere; 1 boe = 1 barrel of oil equivalent = 6 Mcf). For the
208 lowest well site gas production bin of 0 to 29 Mcf/day (i.e, 0 to 0.2 kt of methane production per year) and
209 midstream facilities, we use the empirical absolute methane emission rate data as is. This approach is partly based
210 on the methods used by Omara et al. (2022) for the low production well site category, which exploits a weak
211 relationship between gross gas production data (which is most accessible in empirical measurement studies) and
212 absolute emission rates to better extrapolate emissions to the entire population of production well sites in the
213 CONUS.

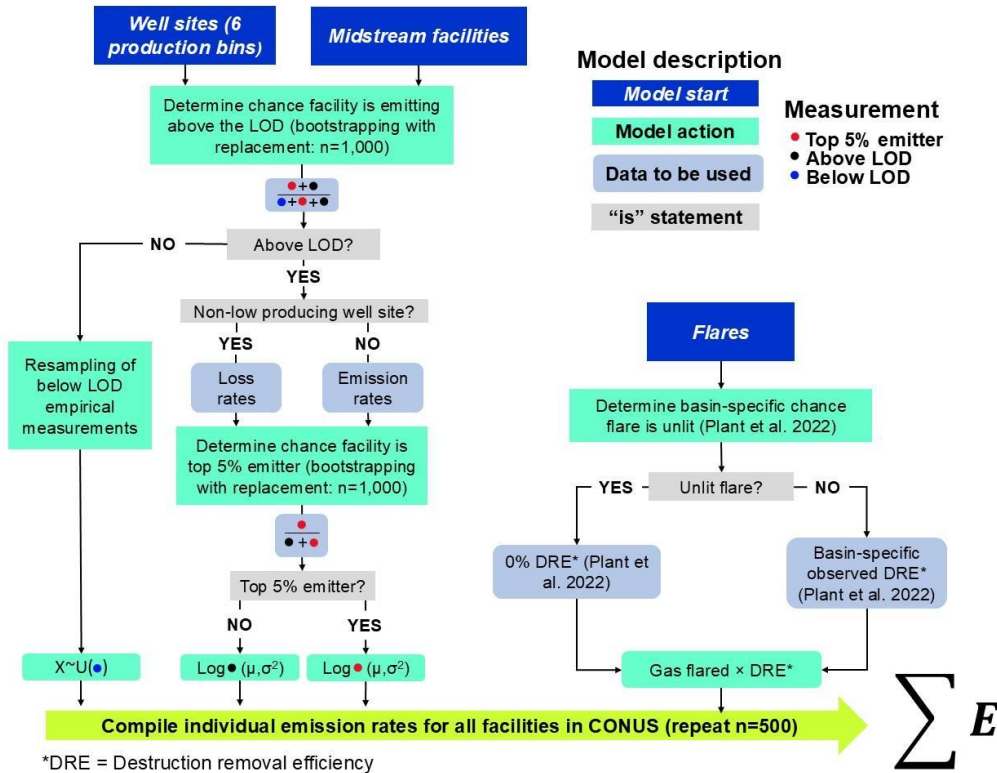
214
$$Loss\ rate = \frac{Emission\ rate\ \left[\frac{kg}{hr}\right]}{\sigma_{CH_4} \times Gas\ production\ \left[\frac{kg}{hr}\right]} \quad (1)$$

215 For our estimation of facility-level emission rates, we break down the modeling process into two separate steps:
216 the first determines whether a randomly selected facility is emitting methane above our method LOD of ≤ 0.1
217 kg/hr/facility, and the second determines the associated methane emission rate for that individual facility. To test the
218 sensitivity of our method to the selection of the method LOD, we also perform an additional sensitivity analysis for
219 other method LODs (Fig. S8). The processes outlined below are all specific to each of our nine facility categories.
220 Brantley et al. (2014) and Lan et al. (2015) are excluded from this first step since they do not include measurements
221 below the method LOD but include valuable data on well site emission rates with associated well site production
222 data. To determine whether a facility is emitting methane above the method LOD threshold in our estimates, we first
223 use bootstrapping with replacement (n=1,000) of our empirical measurement data to [simulate the frequency of](#)
224 [finding determine the chance of](#) an individual facility emitting methane above the method LOD (i.e., ≤ 0.1
225 kg/hr/facility), which we call an “emitting facility” or “emitter” herein (Fig. 2). [The results of the bootstrapping](#)
226 [procedure represent a normal probability distribution from which we estimate the frequency of finding an emitting](#)
227 [facility \(i.e., above the method LOD\) with associated uncertainty bounds. We model the results of the bootstrapping](#)
228 [with replacement as a normal distribution and use the parameters of the modeled distribution to randomly determine](#)
229 [whether a facility is emitting.](#) Next, we remove the empirical measurements below the LOD and use bootstrapping
230 with replacement (n=1,000) on the above LOD empirical measurements to determine the probability of an emitting
231 facility being in the top 5% (i.e., 95th percentile or above of empirical measurement data) or bottom 95% (i.e., 95th
232 percentile or below the empirical measurement data) of emitters, except for processing plants and T&S compressors
233 which had too few measurements (n=20 and n=50 respectively) to distinguish between the top 5% and bottom 95%
234 of emission or loss rates. [Similar to the process of determining the frequency of finding an emitting facility, we use](#)
235 [the results of the bootstrapping to develop a normal probability distribution that classifies an emitting facility as](#)
236 [either a top 5% or bottom 95% emitter.](#) This pseudo-random selection of a top 5% emitter within each facility
237 category accounts for the functional definition of abnormally large emissions (i.e., super-emitters) that can be

238 observed in all facility categories (including well sites in different production bins) (Zavala-Araiza et al. 2015,
239 Brandt et al. 2016). We fit the results of the bootstrapping to two normal distributions: one for the top 5% of emitters
240 and one for the bottom 95% of emitters. We use the associated parameters of each normal distribution to randomly
241 determine whether a facility is emitting in the top 5% or bottom 95% of emitters. These steps are repeated for each
242 facility for each facility category in the CONUS.

243 At the end of the first step of this facility-level modeling process, all facilities in the CONUS are classified as
244 either a: bottom 95% emitter, top 5% emitter, or below the method LOD. [Loss rates are used to calculate emission](#)
245 [rates for the top five highest production bins of well sites, whereas we directly estimate methane emission rates for](#)
246 [the well sites in the lower production cohort \(Fig. 1\), and for midstream facilities excluding VIIRS flare detections.](#)
247 For facilities classified as the top 5% and bottom 95% of emitters, we estimate their methane emissions by first
248 fitting a lognormal distribution to the empirical measurement data, including measurements from Brantley et al.
249 (2014) and Lan et al. (2015), of either the gas production normalized loss rates or methane emission rates (Eq. 1),
250 depending on the facility category. Next, we use the parameters of the modeled distributions to randomly assign
251 either an emission or loss rate to a randomly selected facility (n=500), depending on its emitter status and facility
252 category. We test each estimated methane emission distribution to the associated empirical measurements and find a
253 good fit for all facility categories (Table S6). To account for facilities emitting below the method LOD, we
254 randomly assign an emission rate from re-sampling our dataset of empirical measurements below the method LOD
255 for that facility category. Finally, once all facilities are assigned an emission rate, we compile the ensemble of
256 emission distributions to develop facility-level emission distribution curves and total regional oil/gas methane
257 emissions for the CONUS in 2021.

258 For all VIIRS flares detections, we use the total reported volumes of gas flared for 2021 from flares detected
259 using the VIIRS instrument (Elvidge et al. 2015) multiplied by the observed flare destruction efficiencies and
260 percentage of unlit flares from Plant et al. (2022) to calculate annual methane emission rates from this source. As
261 previously stated, our empirical measurements are largely located outside of oil/gas basins where the majority of
262 VIIRS flare detections are located (i.e. Permian, Eagle Ford, and Bakken), but we cannot discount the possibility
263 that there are instances of double-counting flares measured via our ground-based empirical data and those detected
264 by VIIRS. For each VIIRS flare detection, we randomly determine whether it is an unlit or lit flare based on the
265 basin-specific percentages of unlit flares reported by Plant et al. (2022). If a flare is determined to be lit, we use the
266 corresponding basin-specific observed destruction removal efficiencies as reported by Plant et al. (2022) multiplied
267 by the corresponding annual total volume of gas flared and convert to an emission rate. The basin-specific observed
268 destruction removal efficiencies are estimated through a fitted normal distribution using the mean and standard
269 deviations modeled from the 95% confidence intervals presented in Plant et al. (2022). If a flare is determined to be
270 unlit, we use a destruction removal efficiency of 0%. For VIIRS flare detections located outside of the Bakken,
271 Eagle Ford, and Permian basins, we used the total CONUS averaged destruction removal efficiencies of 95.2%
272 (95% confidence interval: 94.3 – 95.9%) and percentage of unlit flares of 4.1% as reported by Plant et al. (2022).



274

*DRE = Destruction removal efficiency

275
276
277
278

Figure 2: Flowchart describing the facility-level estimates, with steps colored according to the specific process and data being used. We note that methane emission rates for flares are calculated using a separate approach from that of production well sites and midstream facilities. Processing plants and T&S compressors are excluded from the determination of whether a facility is a top 5% emitter due to a lack of available empirical measurement data.

279

2.4 Extrapolation to smaller spatial boundaries

280
281

282

We perform several comparisons of our estimated emission distribution curves and total aggregated emissions to estimates from aerial and satellite remote-sensing studies. [To perform these comparisons, we restrict our estimates and the results from other aerial/satellite studies to spatial domains of interest \(e.g., an oil/gas basin boundary or the overflowed domain from an aerial sampling campaign\), and to specifically compare estimates of oil/gas methane emissions from the facility categories we are investigating in this work.](#) For comparisons to satellite remote-sensing studies, we prioritize national-level satellite inversions that estimate methane emissions from the

287

288 CONUS that include spatially explicit maps of methane emission inversions specifically for oil/gas sources. We join
289 the spatially explicit satellite inversions of methane emissions to the top twelve producing oil/gas basin boundaries
290 in the CONUS, in addition to their national-level inversions which we also use for national comparisons. Since our
291 facility-level model includes geo-located activity data (i.e., facility coordinates), we can estimate facility-level
292 methane emissions distributions and estimate total methane emissions for any spatial boundary in the CONUS by
293 spatially joining facilities within a target boundary. Spatial variability in our facility-level estimates is driven by two
294 main factors: counts of facilities and facility types, and averaged annual production characteristics. Due to
295 constraints on data availability, we do not constrain our available empirical measurement data to the specific regions
296 where they were gathered (Table S3). We tested the sensitivity of excluding empirical measurements gathered from
297 specific oil/gas on the national emission distribution curves and total national methane emissions and found no
298 significant variation (Fig. S9). Due to a lack of data availability, we do not have sufficient spatial information from
299 empirical measurements of G&B compressors, T&S compressors, and processing plants to test for basin-level
300 differences in empirical measurement data.

301 For comparisons to aerial remote sensing studies/results, we prioritize studies that include both measured
302 point sources (i.e., oil/gas methane sources that are above the LOD of the aerial remote sensing measurement
303 platform), estimates of total regional oil/gas emissions, and descriptions/outlines of the surveyed spatial domains
304 which are required for these comparisons. Based on these criteria, we compare our estimated emissions to those
305 from peer-reviewed studies (Cusworth et al., 2022; Kunkel et al., 2023; Xia et al., 2024) and the results of research
306 flights from MethaneAIR in the Permian and Uinta oil/gas basins (Omara et al., 2024; Chan Miller et al., 2023;
307 Chulakadabba et al., 2023; MethaneAIR, 2024), with discussion in later sections on a recent study by Sherwin et al.
308 (2024). In all cases, we estimate facility-level methane emissions within the spatial domains outlined by the aerial
309 remote sensing studies to estimate region-specific methane emission distribution curves, use the relevant method
310 limits of detection to characterize emission rate thresholds valid for comparison, and subtract any emission unrelated
311 to the facility types we characterize (Chen et al., 2024). In the case of Cusworth et al. 2022, we infer the spatial
312 domains by georeferencing figures from their studies using the georeferencer tool QGIS (v.3.34.2-Prizem). We
313 compare our spatially joined facility-level emission distributions to the percentage of emissions contributed from
314 facilities emitting below discrete methane emission rate thresholds for all four aerial remote sensing studies, and to
315 the continuous cumulative methane emissions distribution curves from Bridger GML surveys (Kunkel et al., 2023;
316 Xia et al., 2024).

317 Each aerial remote sensing campaign utilizes independent methods to estimate their percentage
318 contributions from small methane sources, which in some cases requires additional analysis of the aerial remote
319 sensing results. For our analysis of continuous methane emissions distribution curves from the Bridger GML
320 campaigns (Kunkel et al., 2023; Xia et al., 2024), we restrict our analysis to estimated emission ~~rates~~ rates >3
321 kg/hr, which is the approximate LOD of the Bridger GML remote sensing platform. For MethaneAIR, we use the
322 percentage of area emissions (i.e., diffuse area methane sources) relative to the total methane emissions for the
323 spatial boundary, which roughly corresponds to all emissions <200 kg/hr (i.e. effectively those emissions below the

324 point source detection limit of MethaneAIR that flew in multiple campaigns in the US at 40,000ft above ground
325 level (Chulakadabba et al., 2023)). MethaneAIR characterizes the total regional emissions including the spatial area
326 emissions at high resolution using a geostatistical inverse modeling framework (Miller et al., 2013) while ingesting
327 high-emitting point source information in the inversion (Chulakadabba et al., 2023; Omara et al., 2024). For
328 Cusworth et al. (2022), we analyze all campaigns by subtracting both aerially detected pipeline emissions and all
329 non-oil/gas emissions (e.g., wastewater, landfills, agriculture), since our study is focused solely on upstream and
330 midstream oil/gas sources. In addition, we subtract emissions from pipelines and non-oil/gas sources emitting below
331 aerial detection limits (i.e., TROPOMI inversions subtracted by aerially detected emissions) by estimating the
332 relative fractions of pipeline and non-oil/gas sources from the aerial detections, with the assumption that these
333 fractions are representative (Table S4). However, this process can introduce additional uncertainties in our
334 comparisons, especially for campaigns where 50% or more of aerially detected emissions were from pipelines or
335 non-oil/gas sources.

336 We account for the intermittency of detected methane sources with <3 overpasses in Cusworth et al.
337 (2022) by resampling with replacement (n=1,000) the source persistence of methane sources with ≥ 3 overpasses for
338 the same campaign, which is consistent with their methodology. We calculate the percentage contributions of low
339 emitting sources in Cusworth et al. (2022) using Eq. (2): where $\%E_{<x}$ is the percentage of total oil/gas methane
340 emissions below an emission rate threshold x (kg/hr), T is the total area emissions measured via TROPOMI
341 inversions (kg/hr), and $P_{>x}$ is the sum of point source emissions above the emission rate threshold x (kg/hr).

$$342 \quad \%E_{<x} = 1 - \frac{P_{>x}}{T} \quad (2)$$

343 344 **2.5 Uncertainty calculations** 345

346 Our emission distributions based on facility-level estimates incorporate uncertainty through several steps, such
347 as the: probabilistic distributions of a select facility being a top 5%, bottom 95% emitter, or facility emitting below
348 the LOD; emission rate and loss rate distributions produced from facility-level empirical measurements; and flaring
349 combustion efficiencies. In addition, we incorporate uncertainties from the empirical measurements into our facility-
350 level model by simulating new empirical emission rates based on the associated method uncertainties. At the
351 beginning of each of the 500 model iterations, we use the reported empirical methane emission rate data and
352 estimate a new emission rate using a normal distribution with the mean as the initial reported emission rate and the
353 standard deviation as a percentage of the mean value. These measurement uncertainties (i.e., 1-sigma) are chosen
354 based on the measurement methodology using the lower percentage uncertainty ranges provided by Fox et al. (2019)
355 for facilities measured via the OTM-33a ($\pm 25\%$), Gaussian plume dispersion ($\pm 50\%$), and tracer release ($\pm 20\%$)
356 methods. For HiFlow sampler measurements, we use an uncertainty range of $\pm 16\%$ (Riddick et al., 2022), and for
357 chamber-based measurements, we use $\pm 14\%$ (Williams et al., 2023). Therefore, each model iteration incorporates a
358 unique suite of empirical measurement data based on the initially reported emissions and their associated

359 uncertainties, which in turn impacts the probabilistic modeling of the chance of a facility emitting below the method
360 LOD, the empirical data is used to determine the parameters of the lognormal distributions of loss rates and emission
361 rates, and the ranges of the production bins. To calculate the cumulative uncertainty of our facility-level model
362 estimates, we estimate 500 methane emission distributions and aggregate the 2.5th and 97.5th percentiles of our seven
363 primary facility categories (i.e., low and non-low producing well sites, G&B compressors, T&S compressors, and
364 processing plants), which include lit and unlit VIIRS flare detection emissions, to determine our 95% confidence
365 intervals. This process is repeated for all simulations at the national-, basin-, and aerial remote sensing boundary
366 levels. For uncertainty calculations in satellite- and aerial-remote sensing studies we use for comparisons, we present
367 the reported 95% confidence intervals, if available.

368

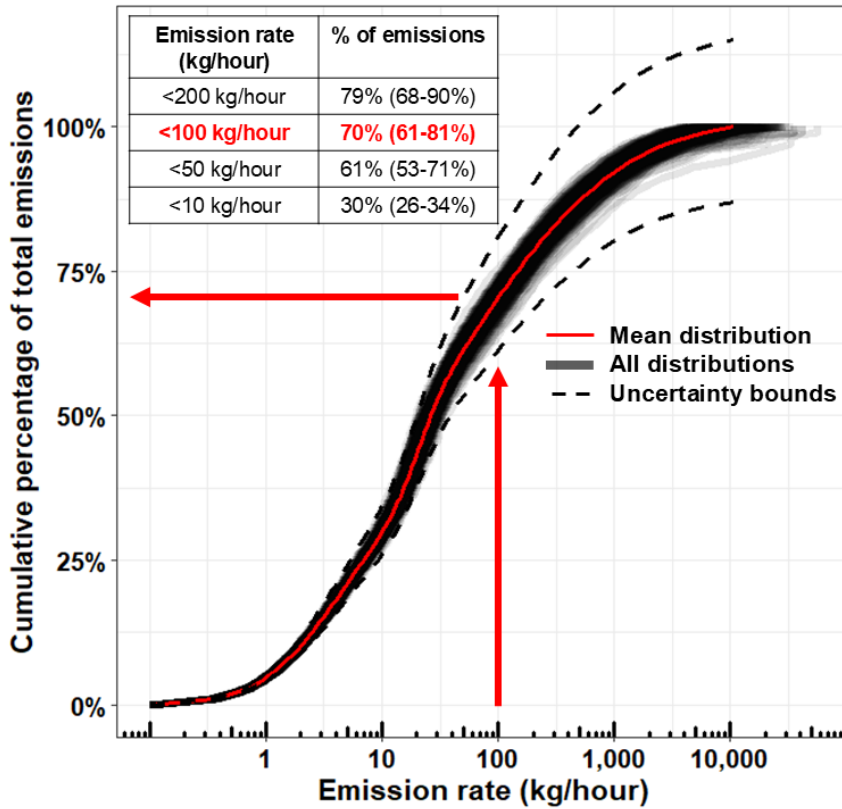
369 **3 Results**

370

371 **3.1 Distribution of emission rates at the national scale**

372

373 Based on the results from our facility-level model estimates, we estimate that 70% (95% confidence
374 interval: 61-81%) of total methane emissions from the upstream/midstream sector in the CONUS for 2021 originate
375 from facilities emitting methane at rates <100 kg/hr (Fig. 3). For other emission rate thresholds, we find that 30%
376 (26-34%) of total emissions come from facilities emitting <10 kg/hr, which corresponds to the lower thresholds of
377 aircraft-based aerial remote sensing studies (Cusworth et al., 2022; Johnson et al., 2021; Kunkel et al., 2023; Thorpe
378 et al., 2024; Xia et al., 2024), and 79% (68-90%) of total emissions come from facilities emitting <200 kg/hr. We
379 find that the emission rate threshold corresponding to 50% of cumulative methane emissions from
380 upstream/midstream facilities in the CONUS for year 2021 is 25 kg/hr (19-33 kg/hr). These results suggest that a
381 large majority of oil/gas emissions in the CONUS are not detectable by existing satellite remote-sensing point



383

384 **Figure 3:** Results from 500 estimated facility-level emission distributions showing the cumulative percentages of
 385 total methane emissions contributed from facilities emitting below methane emission rate thresholds. For example,
 386 facilities emitting <100 kg/hr account for 70% (61-81%) of total methane emissions. The inset table in the upper left
 387 displays the total percentage of methane emissions contributed from several discrete emission rate thresholds with
 388 95% confidence intervals shown in parenthesis.

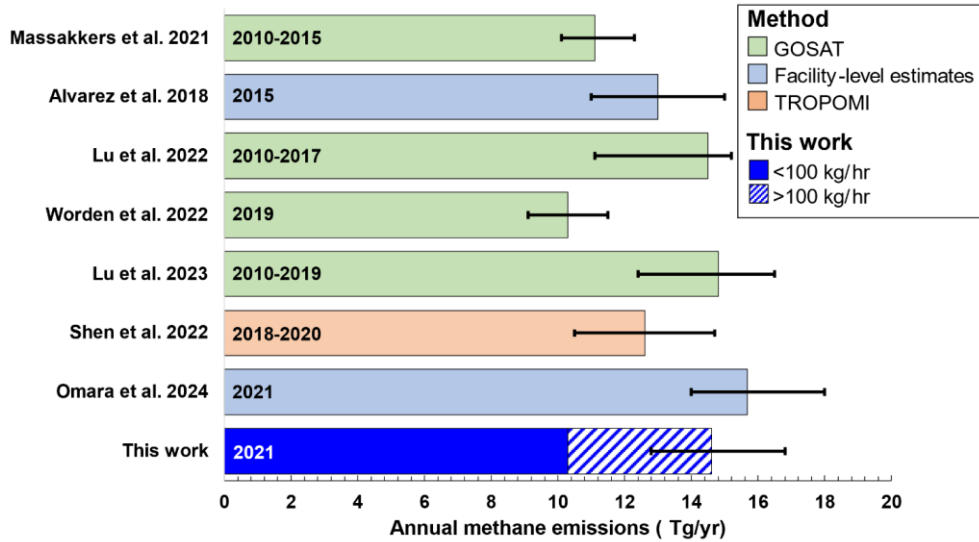
389

390 The distribution for our national-level methane emissions follows an S-shaped curve, noting that the x-axis
 391 (i.e., facility-level methane emission rates) is presented in the \log_{10} scale. From 0.1 to 1 kg/hr, we observe a plateau
 392 in the distribution curve indicating that increasing emission rates within this range do not significantly increase the
 393 percentage contribution to total regional emissions (Fig. 3), similar to the findings in Ravikumar et al. (2019). From 1
 394 to 100 kg/hr, we see a sharper rise in the emission distribution, indicating that increasing emission rates at this range
 395 lead to a more substantial contribution to total methane emissions, and account for 68% (60 – 75%) of total methane

396 emissions (Fig. 3, Table S4). Above an emission rate threshold of 100 kg/hr, we see an exponential decline in the
397 percentage contributions of total emission with increasing emission rates, with total methane emissions in this range
398 amounting to 28% (18 – 37%) of the total oil/gas emissions. Facilities emitting at the 1-10 kg/hr and 100-1,000 kg/hr
399 ranges contribute a similar cumulative percentage at 26% (23 - 29%) and 22% (18 - 26%) respectively. Similar
400 percentage contributions are also observed between the 0.1-1 kg/hr and >1,000 kg/hr ranges at 4.5% (4.0 - 5.1%) and
401 6.1% (2.6 - 13%) respectively. Overall, we find that the highest contribution to total national CONUS methane
402 emissions occurs from facilities emitting in the 10-100 kg/hr range at 42% (37 - 46%). In terms of facility counts,
403 from the 673,940 total active oil/gas facilities we estimate in the CONUS for 2021, we estimate that essentially all
404 (i.e., ~99.9%) of these facilities emit methane below 100 kg/hr.

405 Our facility-level model estimates total methane emissions from US upstream/midstream oil/gas emissions
406 for 2021 to be 14.6 (12.7 - 16.8) Tg/yr, or 1,668,000 (1,453,000 – 1,921,000) kg/hr (Fig. 4), which corresponds to a
407 gross gas production normalized loss rate of 2.4%, assuming a uniform 80% methane content in natural gas across
408 oil/gas producing regions in the CONUS. This national emission total of 14.6 (12.7 - 16.8) Tg/yr is more than
409 double the EPA Greenhouse Gas Inventory Report for natural gas and petroleum systems in 2021, excluding post-
410 meter and distribution methane emissions (Inventory of U.S. Greenhouse Gas Emissions and Sinks, 2024). We
411 compare our total national estimates to previous estimates by seven studies that predominantly utilize satellite-based
412 remote-sensing platforms such as GOSAT and TROPOMI inversions (Lu et al., 2022, 2023; Maasakkers et al.,
413 2021; Shen et al., 2022; Worden et al., 2022) except for Alvarez et al. (2018) and Omara et al. (2024) who developed
414 unique facility-based modeling approaches using empirical measurement data collected from multiple oil/gas basins
415 in the CONUS (Fig. 4). Our estimate of national methane emissions overlaps with six out of seven other national
416 estimates of oil/gas methane emissions for the US, with a combined average of 13.1 (ranging from 11.1 - 15.7)
417 Tg/yr. We do not estimate methane emissions from gathering/transmission/distribution pipelines, post-meter
418 emissions, abandoned oil and gas wells, and refineries due to the scarcity of measurement-based data for these
419 sources. Total methane emissions from these sources emit ~2 Tg/year of methane emissions based on other studies
420 (Williams et al., 2021; Alvarez et al., 2018; Omara et al., 2024; Weller et al., 2020; Inventory of U.S. Greenhouse
421 Gas Emissions and Sinks, 2024). Overall, our total national estimate of CONUS methane emissions for 2021 shows

422 good agreement with multiple independent and recent measurement-based estimates.



423

424 **Figure 4:** Comparison of total CONUS oil/gas emissions for 2021 from this facility-level measurement-based
425 inventory compared to empirical estimates from other studies. Bars are colored according to the methodology used
426 to derive the total national estimates, and the years within the bars represent the corresponding time periods for the
427 estimates. Black inset lines represent 95% confidence intervals. Our total estimates for “This work” do not include
428 emissions from other oil/gas methane sources such as abandoned oil and gas wells,
429 transmission/gathering/distribution pipelines, post-meter emissions, and refineries. Emission estimates from Omara
430 et al. (2024) do not include methane emissions from abandoned oil and gas wells. We assume that the remote
431 sensing estimates (i.e., GOSAT and TROPOMI) include all oil/gas methane sources, including downstream
432 emissions.

433

434 3.2 Distribution of emission rates at the basin-level scale

435

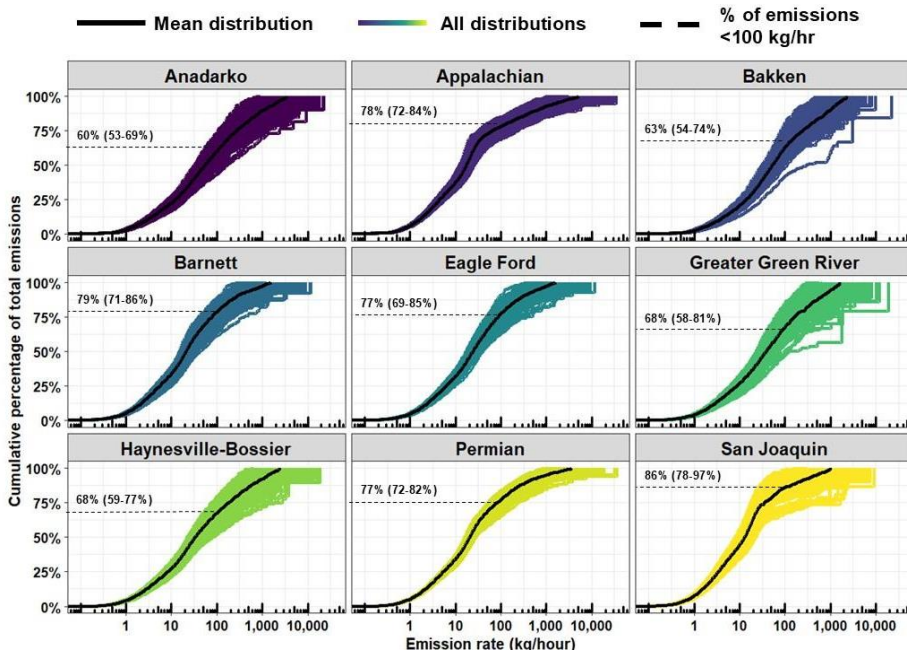
436 Among the top nine emitting oil/gas basins in the CONUS, we observe variations among the different
437 basins in terms of the methane emission distributions, especially at higher emission rate thresholds (Fig. 5). The
438 majority of the top nine emitting oil/gas basins in Fig. 5 show higher percentage contributions from facilities
439 emitting <100 kg/hr when compared to our national estimate of 70% (61 – 81%) (Fig. 3). These percentage
440 contributions vary from ~80% in the Permian, Appalachian, and Eagle Ford basins, up to ~90% in the oil-dominant
441 San Joaquin basin. Only the Anadarko and Bakken basins have notably lower contributions to total emissions at the
442 100 kg/hr threshold at ~60% compared to the national level, which is still a significant majority of total methane
443 emissions. Despite these variations, our facility-level model estimates that the majority of total national oil/gas
444 emissions are consistently contributed from facilities emitting <100 kg/hr for the top nine emitting basins.

445 Our estimated facility-level emission distributions for the top nine emitting oil/gas basins all follow an S-
446 shaped curve (Fig. 5) like the national distribution (Fig. 3), albeit with certain variations. For all basins, the initial
447 plateau in the emissions distribution curves ends at around 1 kg/hr before beginning to rise more steeply. For the
448 Appalachian and San Joaquin basins, the second plateau is at the 20-50 kg/hr emission rate threshold (Fig. 5). For
449 the remaining basins, the rise in the emission distribution curves plateaus gradually, indicating a more consistent
450 relationship of emission rate thresholds to their contribution to total emissions. The variability displayed among the
451 500 basin-level simulations differs among the oil/gas basins, with less spread in the 500 estimated methane
452 emissions distributions for the Appalachian, Anadarko, and Permian basins compared to the Uinta, Denver-
453 Julesburg, and San Joaquin basins (Fig. 5 and Fig. S6). These variations are likely caused in part by the overall total
454 basin-level methane emissions, where an extremely high estimated methane emission rate would have a greater
455 impact on the percentage contribution to the total for basins with lower overall emissions (e.g., the apparent outliers
456 for the Greater Green River and Bakken basins in Fig. 5). We discuss below other plausible causes for basin-to-
457 basin variability in the estimated methane emission distributions.

458 In terms of total methane emissions, the top two emitting oil/gas basins are the Permian and Appalachian,
459 which collectively account for 5.2 (4.4 – 6.3) Tg/year (Fig. S1) or 37% of total upstream and midstream oil/gas
460 methane emissions. This exceeds the cumulative contribution from the other seven highest emitting oil/gas basins
461 which collectively account for 3.7 (2.9 – 5.0) Tg/yr. Notably, we find that the highest emissions in the CONUS
462 occur from regions outside of any basin boundary 4.3 (1.2 – 6.3) Tg/year. Our estimates for basin-level total
463 emissions also show good agreement with remote-sensing satellite-based observations (Fig. S1), except for the
464 Appalachian, Bakken, Greater Green River, and Denver-Julesburg basins where our results are consistently more
465 than double those from the remote-sensing studies that used a prior-emission based inversion result (Lu et al., 2023;
466 Shen et al., 2022). These four basins are in regions with relatively low TROPOMI observation counts and densities
467 compared to other regions in the CONUS (Shen et al., 2022), in addition to other factors that could influence
468 satellite-based inversions such as the presence of many non-oil/gas sources such as coal, livestock, and landfills.
469 Overall, our estimates of total basin-level emissions are consistent with satellite-based observations.

470

471



472
 473 **Figure 5:** A) Results from 500 model simulations showing the cumulative methane emissions distribution curves for
 474 total upstream/midstream oil/gas methane emissions for the top nine emitting oil/gas basins in the CONUS for 2021.
 475 The model averages for each basin are shown in solid black lines. Inset dashed lines represent the percentage
 476 contributions of total emission from sources emitting <100 kg/hr. Emission distribution curves for the remaining
 477 eleven oil/gas basins in the CONUS are shown in Fig. S6, and a map of the spatial boundaries used for the different
 478 oil/gas basins is shown in Fig. S10.

479
 480 **3.3 Distribution of emission rates by facility category**
 481

482 We find significant variations in the methane emission rate distribution curves among the different facility
 483 categories (Fig. 6A). Over 50% of total methane emissions from low (i.e., <15 boe/day, or <0.13 kt of methane
 484 production per year and non-low production well sites, lit flares, and G&B compressor stations occur from facilities
 485 emitting <100 kg/hr (Fig. 6A). In contrast, only 17% (15-18%) of emissions from processing plants, 19% (18-20%)
 486 of emissions from T&S compressor stations, and 9% (7-12%) of emissions from unlit flares are contributed from
 487 emission sources <100 kg/hr. Similar variability is also observed at other emission rate thresholds, such as only 1%
 488 (0-2%) of total emissions for T&S compressor stations, unlit flares, and processing plants originating from facilities
 489 emitting at rates <10 kg/hr, compared to 50% (43-58%) from low producing well sites and 30% (24-35%) from non-
 490 low producing well sites (Fig. 6A). At higher emission rate thresholds, we find that 33% (20-45%) of total emissions
 491 from T&S compressors and processing plants are emitted from facilities <200 kg/hr, compared to 84% (68-93%)

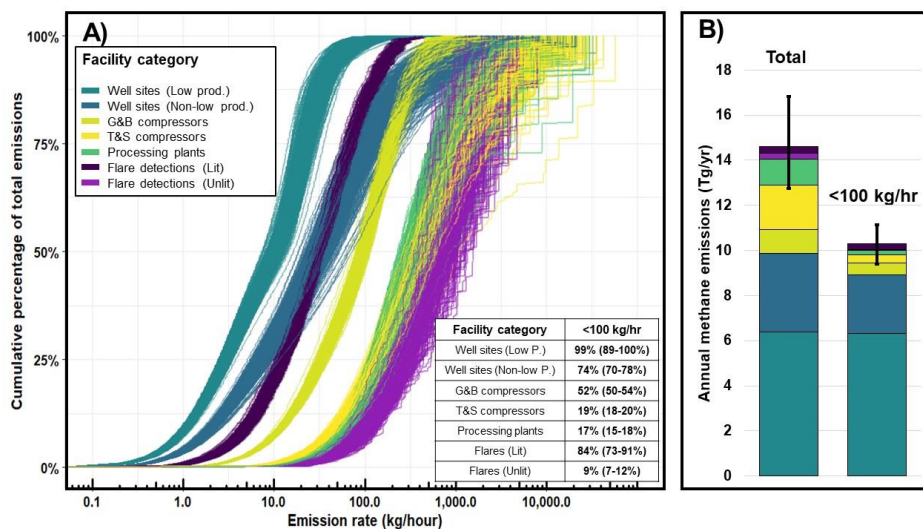
492 from non-low producing well sites (>boe/day of combined oil and gas), 86% (83-88%) from VIIRS flare detections,
493 78% (70-86%) from G&B compressor stations, and essentially 100% of emissions from low producing well sites.

494 A breakdown of the 673,940 total facilities in our model has 541,970 as low-producing well sites, followed
495 by 121,824 non-low-production well sites, 4,431 G&B compressor stations 2,093 T&S compressor stations, 919
496 processing plants, and 3,153 total VIIRS flare detections. Of these 673,940 total facilities, 99.5% (99.4 – 99.6%)
497 emit methane at rates <100 kg/hr (Fig. S11), and in turn contribute 70% of total methane emissions (Fig. 3). Overall,
498 we estimate that 68% of total CONUS oil/gas methane emissions for 2021 come from production well sites, of
499 which 44% are from low-production well sites with combined oil/gas production <15 boe/day (i.e., <0.13 kt of
500 methane production per year), and the remaining 24% from non-low production well sites (i.e., >15 boe/day) (Fig.
501 6B). Midstream facilities contribute 29% of total methane emissions, with 13% from T&S compressors, 8% from
502 processing plants, 7% from G&B compressor stations. The remaining 4% from VIIRS flare detections are evenly
503 split with 2% each from lit and unlit flares respectively. Based on the population counts for each facility category
504 and their corresponding total methane emissions, the average methane emission rate per facility category is highest
505 for processing plants at 146 (115 – 283) kg/hr, followed by 106 (89 – 129) kg/hr for T&S compressor stations, 27
506 (25 - 29) kg/hr for G&B compressor stations, 3.3 (2.9 – 3.8) kg/hr for non-low producing well sites, and 1.3 (1.2 –
507 1.5) kg/hr for low producing well sites. For VIIRS flares detections, we find a large difference in average emissions
508 between lit flares at 11 (9.2 – 13) kg/hr and unlit flares at 205 (132 – 294) kg/hr.

509 Production well sites constitute the bulk of total methane emissions among the facility categories we
510 considered, with most of these emissions contributed from low production well sites. Overall, we find that ~~67-90%~~
511 ~~77% (72-81%)~~ of well site emissions originated from only 10% of national oil and gas production in 2021 (Fig. S7),
512 highlighting a disproportionately large fraction of emissions relative to production. In terms of individual well site
513 level production values, the same ~~77% (72-81%)~~~~67-90%~~ of total cumulative methane emissions were contributed
514 from well sites producing >50 boe/day (i.e., 0.43 kt of methane production per year) or lower. For well sites
515 producing 15 boe/day (i.e., 0.13 kt of methane production per year) or lower, which is the production threshold used
516 to define a well site as being marginally producing in previous work (Deighton et al., 2020; Omara et al., 2022), we
517 find that these low producing well sites accounted for ~~65% (58-69%)~~~~50-75%~~ of total well site emissions, or ~~6.4~~
518 ~~Tg/yr (4.7-6.8 Tg/yr).~~

519

520



521
 522 **Figure 6:** A) Results from an ensemble of 500 estimated methane emission distributions showing the percentage of
 523 total methane emissions among facility categories contributed from facilities emitting at rates below an emission rate
 524 threshold. The inset table on the bottom right displays the discrete percentage contributions to total methane
 525 emissions contributed from facilities emitting <100 kg/hr. B) Breakdown of total annual methane emissions
 526 contributed from all emitting facility categories and those emitting at rates <100 kg/hr.

527
 528 **3.4 Comparisons to aerial remote sensing studies**
 529

530 We perform comparisons of the percentage contributions of methane emissions from facilities emitting
 531 below discrete emission rate thresholds between seven aerial remote sensing campaigns across four distinct regions
 532 and our estimated facility-level results (Fig. 7). The aerial remote sensing technologies include data from Bridger
 533 GML measurements (Kunkel et al., 2023; Xia et al., 2024), MethaneAIR (Omara et al. 2024; Miller et al. 2023), and
 534 the results from Global Airborne Observatory and next-generation Airborne Visible/Infrared Imaging Spectrometer
 535 campaigns (Cusworth et al., 2022) which are also included in the aerial detections used by Sherwin et al. (2024). In
 536 comparing the percentage contributions to total emissions from low-emitting sources between our facility-level
 537 estimates and the aerial remote sensing campaigns, we find that emission contributions agree well across aerial
 538 remote sensing campaigns for the total percentage of methane emissions from facilities emitting, as seen in Fig. 7
 539 for both less than 100 kg/hr and 200 kg/hr.

540 For the Bridger GML remote sensing campaigns (Kunkel et al., 2023; Xia et al., 2024), we find good
 541 agreement in the percentage of total emissions contributed from facilities emitting <200 and <100 kg/hr compared to
 542 our facility-level model estimates (Fig. 7). A comparison of continuous emissions distribution curves between our

543 facility-level emission distributions and two Bridger GML aerial remote sensing campaigns (Kunkel et al., 2023;
544 Xia et al., 2024) targeting four oil/gas basins is shown in Fig. S3. The Bridger GML aerial sampling platform has the
545 lowest LOD among the aerial campaigns we analyze in this work and a similar source resolution (i.e., 30 meters) to
546 our facility-level model (i.e., 50 meters), allowing for a more detailed comparison of continuous emission
547 distribution curves due to the higher number of detected methane sources at low emission rates provided by Bridger
548 GML surveys. We find close agreement between our facility-level methane emission distribution curves and the
549 observed emissions by Bridger GML in the four-basin aggregate provided by Xia et al. (2024) (Fig. S3A) which
550 includes Anadarko, Bakken, Eagle Ford and Permian basins (individual basin data are not currently available in Xia
551 et al. (2024)), as well as separately for the Permian remote sampling campaign (Fig. S3B) by Kunkel et al. (2023),
552 with the measured emissions from the Bridger GML surveys overlapping with our facility-level model simulations
553 throughout the continuous distribution of methane emission rates.

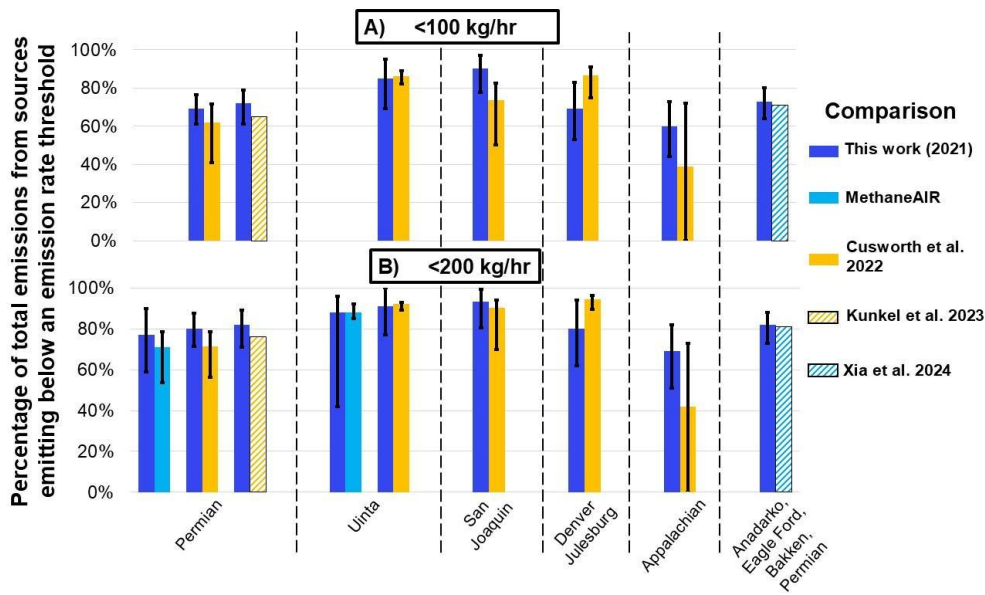
554 For the multiple aerial remote sensing campaigns performed by Cusworth et al. (2022), we generally find
555 good agreement with all of our estimates statistically overlapping for discrete emissions rate thresholds of <100
556 kg/hr and <200 kg/hr for the Permian and Uinta oil/gas basins (Fig. 7). For the San Joaquin and Denver-Julesburg
557 oil/gas basins, we see good agreement at the emission rate threshold of <200 kg/hr and at <100 kg/hr (i.e.
558 overlapping uncertainty bounds). For the Appalachian basin, we find broad agreement at both emission rate
559 thresholds of <100 kg/hr and <200 kg/hr, with our results consistently showing a 20-30% greater contribution from
560 emission sources below the discrete emission rate thresholds (Fig. 7). We find the closest agreement in the Permian
561 and Uinta oil/basins, where the differences in the average percentage contributions vary from -9% to +4% across the
562 three discrete emission rate thresholds of <100 and <200 kg/hr (Fig. 7). In Denver-Julesburg and Appalachian
563 basins, the differences are observed to be larger, compared to other basins, where the differences in average
564 percentage contributions across the discrete emission thresholds vary from -30% to +18%, however, they are within
565 our estimated uncertainty bounds. The detected point sources by Cusworth et al. (2022) in the Denver-Julesburg and
566 Appalachian basins contain many non-oil/gas point sources (Table S4), which may lead to additional uncertainty in
567 the comparisons for these basins since we use the relative proportions of point sources to subtract an estimated
568 contribution of non-oil/gas point sources from the TROPOMI estimates to provide a more direct comparison
569 between our estimates (since our study only focuses on upstream and midstream oil and gas sectors) and those of
570 Cusworth et al. (2022). Notably, the Appalachian basin contains the highest percentage contribution of non-oil/gas
571 point sources at 67% (Table S4). In contrast, we note that all of the detected point sources by Cusworth et al. (2022)
572 in the Permian and Uinta basins were attributed to oil/gas point sources (Table S4).

573 Our comparisons to the available flight results from MethaneAIR, which quantifies both total regional
574 methane emissions and high-emitting point sources >200 kg/hr from the same aerial platform (Chulakadabba et al.,
575 2023), show close agreement between our facility-level estimates and the available aerial campaigns in the Uinta
576 and Permian basins for facilities emitting <200 kg/hr (Fig. 7B). For the MethaneAIR flight in the Uinta basin, we
577 estimate that 92% (46 - 100%) of total oil/gas methane emissions are from sources emitting <200 kg/hr, compared to
578 88% from MethaneAIR (Fig. 7B). For the available flight in the Permian basin from MethaneAIR, we estimate total

579 contributions from sources emitting <200 kg/hr at 77% (59 – 90%) compared to the 71% estimated by MethaneAIR
 580 (Fig. 7B).

581 Overall, our findings show that our facility-level estimates closely agree with the results from multiple
 582 aerial remote sensing campaigns from different regions and using various measurement methods.

583



584

585 **Figure 7:** Comparisons of the cumulative percentage of oil/gas methane emissions from all oil/gas facilities emitting
 586 A) <100 kg/hr, and B) <200 kg/hr, between our facility-level empirical emissions estimates and aerial remote
 587 sensing campaigns. Bars are colored according to the study and grouped according to the target oil/gas basin(s). All
 588 results from the facility-level simulations (i.e., this work) are constrained to the spatial boundaries of the aerial
 589 campaigns for direct comparisons (note that for a given basin, spatial boundaries might be slightly different).
 590 Uncertainty bars for the facility-level simulations are the 2.5th and 97.5th percentiles of 500 simulations. Maps of all
 591 spatial boundaries used for comparisons are provided in Fig. S2. Comparisons to MethaneAIR are not performed at
 592 the <100 kg/hr threshold because MethaneAIR detections are not available for point sources below this emission
 593 rate threshold.

594

595 **4 Discussion**

596

597 Understanding how facilities with different magnitudes of emissions contribute to total regional emissions
598 has direct policy implications for methane quantification and mitigation, such as the selection of
599 measurement/screening methods with the appropriate detection sensitivities (Ravikumar et al., 2018). Our main
600 finding is that 70% of total oil/gas methane emissions from the upstream/midstream sectors come from facilities
601 emitting at rates <100 kg/hr, which is the emission rate threshold above which point source emissions are referred
602 to as “super-emitting” oil/gas source by the EPA (Standards of Performance for New, Reconstructed, and Modified
603 Sources and Emissions Guidelines for Existing Sources: Oil and Natural Gas Sector Climate Review, 2024). While
604 detecting and mitigating emissions from super emitters are important (Cusworth et al., 2022; Duren et al., 2019;
605 Sherwin et al., 2024), our results underscore the need to account for oil/gas methane sources emitting at lower rates,
606 as the cumulative contribution of lower-emitting sites accounts for a large majority of emissions across US oil/gas
607 basins. Facility-level, measurement-based data collected in other countries present a similar story. From a sample of
608 sites (n=302) measured via Bridger GML remote sensing platform in British Columbia, Canada (Tyner and Johnson,
609 2021), roughly 60% of the total quantified oil/gas site-level emissions originate from sites emitting <32 kg/hr. In
610 Romania, a site-level measurement-based inventory (Stavropoulou et al., 2023) using 178 measurements finds that
611 oil production facilities emitting <100 kg/hr contribute 78% of total oil/gas methane emissions in the studied region.
612 In short, the high percentage contribution from lower-emitting (<100 kg/hr) oil/gas facilities that account for a large
613 majority of total emissions is not unique to the US and is likely present in other countries as well. A combination of
614 approaches that characterize entire emission distributions across populations of sites (i.e., not just focusing on
615 measuring super-emitters) and quantification of regional-level emissions is needed in other countries to quantify the
616 relative contributions of low-emitting sources that in aggregate can be significant sources of overall oil/gas methane
617 emissions. Most of our analysis centers around quantifying the percentage contributions of oil/gas methane sources
618 emitting below one discrete emission rate threshold (i.e., <100 kg/hr, per EPA’s definition of a super-emitter). We
619 estimate that over 99% of the total oil/gas facilities that we analyze in this work emit below 100 kg/hr (Fig. S11),
620 which in turn contribute 70% (61 – 81%) of total methane emissions (Fig. 3). The emission rate threshold of 100
621 kg/hr is relevant to US policy decisions (EPA’s Final Rule for Oil and Natural Gas Operations Will Sharply Reduce
622 Methane and Other Harmful Pollution., 2024), but we also illustrate the importance of a complete characterization of
623 emissions, which gains importance as newer methane monitoring technologies have different LODs. For example,
624 the effective LOD at high probabilities of detection for available point source imaging satellites of ~200 kg/hr
625 (Jacob et al., 2022) would only be able to quantify 21% (10-32%) of all oil/gas point sources in the CONUS, if the
626 full oil/gas sector was mapped in its entirety, based on our facility-level results. When considering the relationship
627 of facility-level emission rates to total cumulative methane emissions, we find that oil/gas methane emissions in the
628 CONUS are dominated by many low-emitting facilities, which relates directly to methane measurement
629 technologies.

630 Point source-focused remote sensing platforms offer the advantage of rapidly surveying large areas (i.e.,
631 100’s-1,000’s km²) which facilitates the detection and quantification of high-emitting point sources (Cusworth et al.,
632 2022; Duren et al., 2019; Sherwin et al., 2024). In contrast, logistical constraints often limit the sample sizes for
633 ground-based vehicle sampling platforms, however, these limitations can be overcome with stratified random,

634 representative sampling and statistical analysis approaches like this work. Ground-based measurement platforms
635 provide much lower LODs (i.e., <1 kg/hr) when compared to remote sensing platforms, which are necessary to
636 quantify emissions from the large number of small methane sources we find that contribute roughly three-quarters of
637 total regional oil/gas emissions in the CONUS and will only improve as additional ground-based measurements are
638 gathered. Overall, our main findings highlight the importance of methods that can rapidly locate the small number of
639 high-emitting point sources we estimate, but our findings emphasize the need to account for the disproportionately
640 large majority percentage of total regional oil/gas emissions that are emitted from smaller diffuse methane sources.

641 When extrapolating our facility-level model results to the basin-level we see variations among the emission
642 distribution curves for different oil/gas basins, but still find that most methane emissions come from facilities
643 emitting <100 kg/hr. The variations in the emission distribution curves for different basins are driven by many
644 factors, such as the: production characteristics, number and density of facilities, different types and relative counts of
645 facility categories, the availability of empirical measurement data used to model emissions, and the total oil/gas
646 methane emissions (i.e., the denominator). For example, the Appalachian basin is dominated by a high number of
647 older low-production well sites (Deighton et al., 2020; Riddick et al., 2019; Enverus, 2024) with fewer midstream
648 facilities such as processing plants and G&B compressors, which contrasts with the Bakken basin where we find a
649 high number of midstream facilities, high-producing well sites, and VIIRS flare detections (Elvidge et al., 2015;
650 Enverus, 2024). When comparing the emissions distribution curves for the Bakken and Appalachian basins (Fig. 5),
651 we observe higher contributions from lower-emitting facilities for the Appalachian compared to the Bakken. An
652 example of differences in basin-level production is shown in Fig. S4 and Fig. S5, where we see variable profiles
653 among the different oil and gas-producing basins in terms of well site production characteristics, which are the main
654 source of total methane emissions in this work (Fig. 6). We also observe the influence of total basin-level emissions
655 on the variability among our emission distribution curves, where large emitting sources in the San Joaquin basin can
656 lead to high variability among the estimated emission distribution curves compared to the Permian basin which has
657 roughly ten times the total emissions compared to the San Joaquin (Fig. 5). We note that a direct comparison of our
658 model results with aerial remote sensing methods may be limited, in part, by methodological differences in methane
659 quantification approaches (and underlying uncertainties). The remote sensing observations assessed here as
660 snapshots may capture facility-level emission distributions that are not well represented in annually averaged
661 methane emissions distributions, as we estimate here. Nevertheless, we find broad agreement with these independent
662 aerial remote sensing estimates at the basin scale and across smaller spatial domains, as discussed. Ultimately, as
663 many characteristics will influence methane emissions distribution curves among different oil/gas producing regions
664 in the CONUS, mitigation strategies will need to be structured accordingly to the region they are targeting.

665 Our results find that over half of cumulative methane emissions from three different facility categories
666 come from facilities emitting <100 kg/hr, including methane emissions from lit and unlit flares. We show how the
667 large contributions from small methane sources to total regional emissions are not unique to any one facility
668 category, but it is important to contextualize our emission distribution curves with the corresponding total regional
669 emissions. Our facility-level estimates find that the main source of oil/gas methane emissions in the CONUS are

670 oil/gas production well sites, of which the low production category is responsible for 44% (39 – 49%) of the total
671 estimated oil/gas methane emissions in the CONUS in 2021. Low-producing well sites, also known as “marginal
672 wells”, have been shown in previous work to be a significant source of methane emissions, especially relative to
673 their contribution to overall oil/gas production (Deighton et al., 2020; Omara et al., 2022). Omara et al. (2022) found
674 that marginal wells contributed anywhere from 37%-75% of total methane emissions from production well sites,
675 which is like our estimates (i.e., 50-7565%). Despite low production well sites having a lower mean emission rate
676 compared to other facility categories, the large facility counts result in significant aggregate total emissions of
677 methane. This implies that detection and mitigation strategies to reduce methane emissions from these and other
678 low-emitting oil and gas infrastructure (e.g., abandoned oil/gas wells) would require alternative mitigation and
679 detection approaches compared to those for the small number of super-emitting emission sources. For detection,
680 measurement methods that can measure emission rates between 0.1-100 kg/hr are required, since this range makes
681 up 70% of total methane emissions (Figure 3 and Table S1) as modeled herein. In terms of methane mitigation
682 policy, financial incentives, like the USD 4.7 billion from the Biden Bipartisan Infrastructure Law for abandoned
683 wells, could be used to prioritize the repair of old and leak-prone production well sites, as these low-producing well
684 sites only account for a small fraction (i.e., 5.6% in 2019) of total oil/gas production (Omara et al., 2022).

685 We see good agreement between our facility-level results and a majority of aerial remote sensing studies, which
686 are expected to capture a wide range of high-emitting facilities in a survey region. For example, when comparing
687 our model results to Kunkel et al. (2023) and Xia et al. (2024) we find that our estimated methane emissions closely
688 match the distribution of methane emissions measured in Bridger GML surveys (Fig. S3). We also find good
689 agreement to satellite remote sensing estimates of emissions, such as our basin-level (Fig. S1) and national-level
690 comparison to satellite inversions (Fig. 3), and other aerial remote sensing study regions (Table S2). Our
691 comparisons of the contributions of low-emitting sources below discrete emission rate thresholds also agree closely
692 with recent MethaneAIR, Kairos Aerospace, GAO, and AVIRIS-NG aerial surveys, whose results also highlight the
693 importance of small methane sources to overall oil/gas methane emissions. Recently, Sherwin et al. (2024)
694 suggested that a majority of total emissions originate from a small fraction of high-emitting sites. Notably, most of
695 the aerial measurements that are used in Sherwin et al. (2024) are obtained from the Cusworth et al. (2022) study,
696 with which we see good agreement (Fig. 7). Sherwin et al. (2024) perform an alternative analysis than Cusworth et
697 al. (2022) for aerially measured sources with <3 overpasses and assume that sources with one or two overpasses
698 emit at their observed intermittency of 100%, 50%, or 0% of the time. This difference in analytical approaches
699 produces higher contributions from aerial emissions in Sherwin et al. (2024) by 31% on average for seven aerial
700 campaigns compared to Cusworth et al. (2022) (Table S7), which uses a resampling approach described earlier in
701 the Methods Section 2.4. In addition, emissions from Sherwin et al. (2024) that are below aerial detection limits are
702 estimated using a combination of an equipment-level bottom-up model presented in Rutherford et al. (2021) for
703 production well sites, and emission factors from the U.S. Greenhouse Gas Inventory (Inventory of U.S. Greenhouse
704 Gas Emissions and Sinks, 2024) for midstream facilities, which produces 52% lower emissions on average for seven
705 aerial campaigns (Table S7). Therefore, the aerially measured emissions in Sherwin et al. (2024) are higher and the
706 emissions below aerial detection limits are lower which leads to a higher contribution to total methane emissions

707 from high-emitting facilities (Table S7). Ultimately, the broad agreement we find across multiple disparate
708 measurement techniques and platforms across Bridger GML aerial campaigns (Kunkel et al., 2023; Xia et al., 2024),
709 MethaneAIR measurements (MethaneAIR L4 Area Sources 2021 | Earth Engine Data Catalog, 2024; Omara et al.,
710 2024), and the multiple surveyed regions presented in Cusworth et al. (2022), altogether provide collective evidence
711 about the large contribution of smaller emission sources to total regional emissions.

712 Given the variability in methane detection technologies, a range of approaches can be taken to estimate methane
713 emission rate distributions, each providing unique advantages and disadvantages. MethaneAIR provides a novel
714 remote sensing approach where high-emitting point sources, distributed area sources and total regional emissions are
715 quantified using the same aerial platform, providing the ability to directly measure high-emitting point source and
716 diffuse area contributions to total regional estimates. In the work by Xia et al. (2024) they combine measurements
717 from Bridger GML across four oil/gas basins and use component-level simulations to account for facilities emitting
718 below the 3 kg/hr LOD of Bridger GML. Other approaches also exist, such as Cusworth et al. (2022) who combine
719 TROPOMI inversions to estimate total regional methane emissions with point source emissions quantified from their
720 aerial detection platforms (i.e., GAO, AVIRIS-NG). Similarly, Sherwin et al. (2024) combine point source emissions
721 measured via aerial remote sensing with site/facility-level emission rates estimates calculated from a combination of
722 an equipment-level bottom-up model for production well sites (Rutherford et al., 2021) and emission factors from the
723 2023 GHGI for midstream facilities (Inventory of U.S. Greenhouse Gas Emissions and Sinks, 2024) for facilities
724 emitting below aerial detection limits. Remote sensing studies have key advantages over ground-based sampling
725 platforms, such as rapidly surveying wide areas and capturing higher-emitting point sources, but have variable LODs
726 depending on the target region, topography, measurement technology, presence of co-located non-oil/gas methane
727 sources (i.e., source attribution), weather conditions, infrastructure density, and infrastructure type(s). These variables
728 pose additional challenges when quantifying the contributions from facilities emitting above/below specific emission
729 rate thresholds, which are critical information to inform mitigation policy. Assessing performance, tracking mitigation,
730 and accurate reporting requires building a comprehensive picture of emissions by characterizing all emitters big and
731 small, and reconciling with total basin/sub-basin level emissions. Ultimately, the key seems to be merging the best
732 data from both approaches to build a hybrid inventory, ideally using a multi-tiered system with multiple methods that
733 span a range of LODs that allow for gathering empirical measurements from facilities emitting at all parts of the
734 methane emission distribution curve. Our study is a step in that direction considering measurement-based data while
735 presenting a robust comparison with available independent remote sensing measurements. At the same time, large-
736 area aggregate emissions data obtained from wide-area remote sensing mapping or mass balance surveys can better
737 constrain total regional emissions (e.g. Cusworth et al. 2022; Omara et al. 2024) towards a more empirically robust
738 denominator in characterizing the relative contributions of small emission and high emission sources to total
739 emissions.

740 We show that our facility-level emission models produce national- and basin-level methane emissions estimates
741 that are in good agreement with other independent measurement-based studies. However, we note the following
742 limitations/biases that could be improved with future data collection efforts. The empirical measurements that we

743 use in our model are representative of the year and time they were measured (i.e., 2010-2020), meaning that they
744 would not reflect any updates in regulatory practices or changes in facility operational and emission management
745 practices. In addition, there are variations in the number of production well site empirical measurements among
746 oil/gas basins (Table S3) although a sensitivity analysis shows that excluding data from individual oil/gas basins
747 does not significantly impact our results (Fig. S9). Furthermore, there are several oil/gas methane emission sources
748 that we do not account for in our estimates, which include: gathering/transmission/distribution pipelines, oil refining
749 and transportation, abandoned oil/gas wells, offshore oil/gas infrastructure, post-meter sources, and oil/gas
750 distribution infrastructure in urban areas. For some sources omitted in this work such as abandoned oil/gas wells,
751 their inclusion would likely lead to a higher contribution from low-emitting facilities, since the highest recorded
752 emission rate from an abandoned oil/gas well is 76 kg/hr (Riddick et al., 2024). For others such as oil refineries,
753 their inclusion would likely lead to a lower contribution from small methane sources given their low facility counts
754 and high per-site emissions (Duren et al., 2019). Despite their omissions, total methane emissions from these sources
755 are currently estimated to account for 5-10% (Alvarez et al., 2018; Riddick et al., 2024; Inventory of U.S.
756 Greenhouse Gas Emissions and Sinks, 2024; Williams et al., 2021) of total oil/gas sectoral emissions. Our estimates
757 also utilize empirically measured emission rates from ground-based sampling platforms which are limited in
758 number, especially in the case of processing plants (n=20) and T&S compressor stations (n=50) (Table S2). The
759 empirical data used in our analysis includes a smaller sample of super-emitting facilities relative to those captured
760 by remote sensing platforms (Duren et al., 2019; Sherwin et al., 2024), but our use of production-normalized loss
761 rates and lognormal distributions to estimate facility-level methane emission rates anticipates and accounts for the
762 possibility of finding low-probability, high-magnitude emissions that occur at rates beyond those that appear in our
763 dataset of empirical observations. For example, our highest empirical emission rate is 1,360 kg/hr for a T&S
764 compressor station, whereas our maximum estimated facility-level emission rate across all 500 facility-level
765 emission distribution curves averages 7,500 kg/hr (3,000 - 21,000 kg/hr). Finally, we include a small number (i.e.,
766 5% of total empirical data used in the model) of measurements for production well-sites gathered using ground-
767 based component/source-level sampling methods from two studies (Deighton et al., 2020; Riddick et al., 2019). All
768 measurements from these two studies targeted the lowest production cohort of production well sites and exhibited
769 statistically lower emission rates than those gathered using facility-level ground-based methods for the same well
770 site production cohort, meaning that any bias introduced by the inclusion of these measurements would lead towards
771 the underestimation of total emissions and/or the percentage contributions from low-emitting sources. Despite these
772 limitations, we have shown that our results are broadly in agreement with satellite- and aerial-based remote sensing
773 studies at national/basin/local scales, and other facility-level estimates.

774 Going forward, several approaches can be used to better understand the percentage contributions from facilities
775 emitting at different leak rate thresholds, and ultimately improve our understanding of oil/gas methane emissions in
776 the CONUS and around the world. A combination of multiple satellite and aerial remote sensing approaches and
777 synthesis of their data by bringing in point source detections at multiple thresholds at the same time characterizing
778 total regional emissions as demonstrated using a compilation of multi-scale measurements seems a viable pathway
779 towards building a more complete picture of the overall methane emissions. Combining aerial and satellite remote

780 sensing measurements with ground-based site/facility-level estimates presents itself as an effective next step, as
781 implemented/suggested by prior studies (Allen, 2014; Alvarez et al., 2018). Aerial or satellite remote sensing
782 platforms focused on point source detection offer the ability to rapidly locate the small number of the highest
783 emitting facilities that contribute a disproportionate fraction of emissions, offering valuable data on specific facility
784 locations that allow for rapid mitigation. However, more direct observational approaches are needed to acquire total
785 emissions data which according to this study is dominated by small-emitting sources that are undetected by high-
786 emitting point source detection systems. Facility-level population-based approaches can account for the lower-
787 emitting facilities that contribute the most total oil/gas methane emissions, which is needed for accurate emission
788 reporting and understanding the contributions of total emissions above/below emission rate thresholds. The ground-
789 based estimates can be further constrained by large-area aggregated emission quantification provided by regional
790 remote sensing or mass balance mapping approaches (Shen et al., 2022; Omara et al., 2024; Jacob et al., 2022)
791 towards producing a more robust overall emission quantification.

792 5 Conclusions

793 In conclusion, our work highlights several key aspects of oil/gas methane emission rate distribution curves
794 in the CONUS for 2021, which include:

- 795 1. A large majority (70%) of total national continental oil/gas methane emissions in the US originate from
796 lower-emitting facilities (<100 kg/hr).
- 797 2. Emission rate distributions vary among different oil/gas basins, but among the top nine producing basins
798 we consistently find that most methane emissions (60%-86%) originate from oil/gas facilities emitting at
799 rates <100 kg/hr.
- 800 3. Production well sites were found to be responsible for 70% of regional oil/gas methane emissions, from
801 which the sites that accounted for only 10% of national oil and gas production in 2021, disproportionately
802 accounted for ~~77%~~ (7267-9081%) of the total well site emissions.
- 803 4. Our results were consistently found to be in close agreement with those from independent aerial/satellite
804 remote sensing estimates, both in comparing contributions from discrete emission rate thresholds and
805 continuous emissions distribution curves, which emphasize the importance of the large majority
806 contribution of small-emitting methane sources to total oil/gas methane emissions.

807 Our results highlight, and quantify, the significant contributions of the large number of low-emitting oil/gas
808 facilities to total regional/basin/local oil/gas methane emissions in the CONUS for 2021. In addition to the CONUS,
809 the small oil/gas methane sources are likely a significant component of total regional emissions in other countries as
810 well as recent data suggest from Romania and Canada (Stavropoulou et al., 2023; Tyner and Johnson, 2021) and
811 would need to be further investigated to build a comprehensive assessment of small-emitting methane emissions and
812 their relative contributions to total oil/gas methane emissions globally. This work emphasizes the need for multi-

813 scale approaches to quantify total regional oil/gas methane emissions; and at the same time characterize and account
814 for the large contribution from small emission sources dispersed across a wide area, in addition to incorporating data
815 on high-emitting point sources towards producing overall robust methane emission quantification.

816
817 **Data availability**

818 All 500 full emission rate distributions at the national level are available to download from Zenodo (link:
819 <https://doi.org/10.5281/zenodo.13314532>). All estimated methane emission rate distributions at the basin or small
820 target scale are available upon request. Empirical measurement data used in the estimation of the methane emission
821 distribution curves are available from the references listed in Table S2.

822
823 **Code availability**

824 R code used to create the methane emission distribution curves and figures is available upon reasonable request.

825
826 **Acknowledgements**

827 We acknowledge funding support from the Bezos Earth Fund. We would like to thank Jack Warren for his valuable
828 efforts in analyzing point source emissions from MethaneAIR aerial campaigns.

829
830 **Author contributions**

831 JPW and RG designed this study. JPW created the code used to produce all results, with inputs from MO, KM, DZA,
832 and AH. MethaneAIR analysis was provided by JB, MS, and SW. Multi-sensor airborne intercomparison was
833 performed by JPW and RG. JPW prepared the manuscript with input from all co-authors.

834
835 **Competing interests**

836 The authors declare that they have no conflict of interest.

837
838 **References**

839 Allen, D. T.: Methane emissions from natural gas production and use: reconciling bottom-up and top-down
840 measurements, *Current Opinion in Chemical Engineering*, 5, 78–83, <https://doi.org/10.1016/j.coche.2014.05.004>,
841 2014.

842 Alvarez, R. A., Zavala-Araiza, D., Lyon, D. R., Allen, D. T., Barkley, Z. R., Brandt, A. R., Davis, K. J., Herndon, S.
843 C., Jacob, D. J., Karion, A., Kort, E. A., Lamb, B. K., Lauvaux, T., Maasackers, J. D., Marchese, A. J., Omara, M.,
844 Pacala, S. W., Peischl, J., Robinson, A. L., Shepson, P. B., Sweeney, C., Townsend-Small, A., Wofsy, S. C., and
845 Hamburg, S. P.: Assessment of methane emissions from the U.S. oil and gas supply chain, *Science*, 361, 186–188,
846 <https://doi.org/10.1126/science.aar7204>, 2018.

Formatted: Bibliography, Space After: 0 pt, Line spacing:
single, Border: Top: (No border), Bottom: (No border), Left:
(No border), Right: (No border), Between : (No border)

847 Enverus | Creating the future of energy together.: <https://www.enverus.com/>, last access: 25 March 2024.

848 Standards of Performance for New, Reconstructed, and Modified Sources and Emissions Guidelines for Existing
849 Sources: Oil and Natural Gas Sector Climate Review: <https://www.federalregister.gov/documents/2024/03/08/2024-00366/standards-of-performance-for-new-reconstructed-and-modified-sources-and-emissions-guidelines-for>, last
850 access: 22 July 2024.

851

852 AR6 Synthesis Report: Climate Change 2023: <https://www.ipcc.ch/report/ar6/syr/>, last access: 6 March 2024.

853 MethaneAIR L4 Area Sources 2021 | Earth Engine Data Catalog: [https://developers.google.com/earth-
854 engine/datasets/catalog/EDF_MethaneSAT_MethaneAIR_methaneair-L4area-2021](https://developers.google.com/earth-engine/datasets/catalog/EDF_MethaneSAT_MethaneAIR_methaneair-L4area-2021), last access: 27 March 2024.

855 Brandt, A. R., Heath, G. A., and Cooley, D.: Methane Leaks from Natural Gas Systems Follow Extreme Distributions,
856 *Environ. Sci. Technol.*, 50, 12512–12520, <https://doi.org/10.1021/acs.est.6b04303>, 2016.

857 Brantley, H. L., Thoma, E. D., Squier, W. C., Guven, B. B., and Lyon, D.: Assessment of Methane Emissions from
858 Oil and Gas Production Pads using Mobile Measurements, *Environ. Sci. Technol.*, 48, 14508–14515,
859 <https://doi.org/10.1021/es503070q>, 2014.

860 Caulton, D. R., Lu, J. M., Lane, H. M., Buchholz, B., Fitts, J. P., Golston, L. M., Guo, X., Li, Q., McSpirt, J., Pan,
861 D., Wendt, L., Bou-Zeid, E., and Zondlo, M. A.: Importance of Superemitter Natural Gas Well Pads in the Marcellus
862 Shale, *Environ. Sci. Technol.*, 53, 4747–4754, <https://doi.org/10.1021/acs.est.8b06965>, 2019.

863 Chan Miller, C., Roche, S., Wilzewski, J. S., Liu, X., Chance, K., Souri, A. H., Conway, E., Luo, B., Samra, J.,
864 Hawthorne, J., Sun, K., Staebell, C., Chulakadabba, A., Sargent, M., Benmergui, J. S., Franklin, J. E., Daube, B. C.,
865 Li, Y., Laughner, J. L., Baier, B. C., Gautam, R., Omara, M., and Wofsy, S. C.: Methane retrieval from MethaneAIR
866 using the CO₂ Proxy Approach: A demonstration for the upcoming MethaneSAT mission, *EGUsphere*, 1–40,
867 <https://doi.org/10.5194/egusphere-2023-1962>, 2023.

868 Chen, Y., Sherwin, E. D., Berman, E. S. F., Jones, B. B., Gordon, M. P., Wetherley, E. B., Kort, E. A., and Brandt, A.
869 R.: Quantifying Regional Methane Emissions in the New Mexico Permian Basin with a Comprehensive Aerial Survey,
870 *Environ. Sci. Technol.*, 56, 4317–4323, <https://doi.org/10.1021/acs.est.1c06458>, 2022.

871 Chen, Y., Sherwin, E. D., Wetherley, E. B., Yakovlev, P. V., Berman, E. S. F., Jones, B. B., Hmiel, B., Lyon, D. R.,
872 Duren, R., Cusworth, D. H., and Brandt, A. R.: Reconciling ultra-emitter detections from two aerial hyperspectral
873 imaging surveys in the Permian Basin, 2024.

874 Chulakadabba, A., Sargent, M., Lauvaux, T., Benmergui, J. S., Franklin, J. E., Chan Miller, C., Wilzewski, J. S.,
875 Roche, S., Conway, E., Souri, A. H., Sun, K., Luo, B., Hawthorne, J., Samra, J., Daube, B. C., Liu, X., Chance, K.,
876 Li, Y., Gautam, R., Omara, M., Rutherford, J. S., Sherwin, E. D., Brandt, A., and Wofsy, S. C.: Methane point source
877 quantification using MethaneAIR: a new airborne imaging spectrometer, *Atmospheric Measurement Techniques*, 16,
878 5771–5785, <https://doi.org/10.5194/amt-16-5771-2023>, 2023.

879 Cusworth, D. H., Thorpe, A. K., Ayasse, A. K., Stepp, D., Heckler, J., Asner, G. P., Miller, C. E., Yadav, V., Chapman,
880 J. W., Eastwood, M. L., Green, R. O., Hmiel, B., Lyon, D. R., and Duren, R. M.: Strong methane point sources
881 contribute a disproportionate fraction of total emissions across multiple basins in the United States, *Proceedings of
882 the National Academy of Sciences*, 119, e2202338119, <https://doi.org/10.1073/pnas.2202338119>, 2022.

883 Deighton, J. A., Townsend-Small, A., Sturmer, S. J., Hoschouer, J., and Heldman, L.: Measurements show that
884 marginal wells are a disproportionate source of methane relative to production, *Journal of the Air & Waste
885 Management Association*, 70, 1030–1042, <https://doi.org/10.1080/10962247.2020.1808115>, 2020.

886 Duren, R. M., Thorpe, A. K., Foster, K. T., Rafiq, T., Hopkins, F. M., Yadav, V., Bue, B. D., Thompson, D. R.,
887 Conley, S., Colombi, N. K., Frankenberg, C., McCubbin, I. B., Eastwood, M. L., Falk, M., Herner, J. D., Croes, B. E.,
888 Green, R. O., and Miller, C. E.: California’s methane super-emitters, *Nature*, 575, 180–184,
889 <https://doi.org/10.1038/s41586-019-1720-3>, 2019.

890 -Elvidge, C. D., Zhizhin, M., Baugh, K., Hsu, F.-C., and Ghosh, T.: Methods for Global Survey of Natural Gas Flaring
891 from Visible Infrared Imaging Radiometer Suite Data, *Energies*, 9, 14, <https://doi.org/10.3390/en9010014>, 2016.

892 ERG: City of Fort Worth Natural Gas Air Quality Study, Final Report, Eastern Research Group, Inc. (ERG), 2011.

893

894 Fox, T. A., Barchyn, T. E., Risk, D., Ravikumar, A. P., and Hugenholtz, C. H.: A review of close-range and screening
895 technologies for mitigating fugitive methane emissions in upstream oil and gas, *Environ. Res. Lett.*, 14, 053002,
896 <https://doi.org/10.1088/1748-9326/ab0cc3>, 2019.

897 Goetz, J. D., Floerchinger, C., Fortner, E. C., Wormhoudt, J., Massoli, P., Knighton, W. B., Herndon, S. C., Kolb, C.
898 E., Knipping, E., Shaw, S. L., and DeCarlo, P. F.: Atmospheric Emission Characterization of Marcellus Shale Natural
899 Gas Development Sites, *Environ. Sci. Technol.*, 49, 7012–7020, <https://doi.org/10.1021/acs.est.5b00452>, 2015.

900 de Gouw, J. A., Veeffkind, J. P., Roosenbrand, E., Dix, B., Lin, J. C., Landgraf, J., and Levelt, P. F.: Daily Satellite
901 Observations of Methane from Oil and Gas Production Regions in the United States, *Sci Rep*, 10, 1379,
902 <https://doi.org/10.1038/s41598-020-57678-4>, 2020.

903 Jacob, D. J., Varon, D. J., Cusworth, D. H., Dennison, P. E., Frankenberg, C., Gautam, R., Guanter, L., Kelley, J.,
904 McKeever, J., Ott, L. E., Poulter, B., Qu, Z., Thorpe, A. K., Worden, J. R., and Duren, R. M.: Quantifying methane
905 emissions from the global scale down to point sources using satellite observations of atmospheric methane,
906 *Atmospheric Chemistry and Physics*, 22, 9617–9646, <https://doi.org/10.5194/acp-22-9617-2022>, 2022.

907 Johnson, M. R., Tyner, D. R., and Szekeres, A. J.: Blinded evaluation of airborne methane source detection using
908 Bridger Photonics LiDAR, *Remote Sensing of Environment*, 259, 112418, <https://doi.org/10.1016/j.rse.2021.112418>,
909 2021.

910 Kunkel, W. M., Carre-Burritt, A. E., Aivazian, G. S., Snow, N. C., Harris, J. T., Mueller, T. S., Roos, P. A., and
911 Thorpe, M. J.: Extension of Methane Emission Rate Distribution for Permian Basin Oil and Gas Production
912 Infrastructure by Aerial LiDAR, *Environ. Sci. Technol.*, 57, 12234–12241, <https://doi.org/10.1021/acs.est.3c00229>,
913 2023.

914 Lan, X., Talbot, R., Laine, P., and Torres, A.: Characterizing Fugitive Methane Emissions in the Barnett Shale Area
915 Using a Mobile Laboratory, *Environ. Sci. Technol.*, 49, 8139–8146, <https://doi.org/10.1021/es5063055>, 2015.

916 Lu, X., Jacob, D. J., Wang, H., Maasackers, J. D., Zhang, Y., Scarpelli, T. R., Shen, L., Qu, Z., Sulprizio, M. P.,
917 Nesser, H., Bloom, A. A., Ma, S., Worden, J. R., Fan, S., Parker, R. J., Boesch, H., Gautam, R., Gordon, D., Moran,
918 M. D., Reuland, F., Villasana, C. A. O., and Andrews, A.: Methane emissions in the United States, Canada, and
919 Mexico: evaluation of national methane emission inventories and 2010–2017 sectoral trends by inverse analysis of in
920 situ (GLOBALVIEWplus CH₄ ObsPack) and satellite (GOSAT) atmospheric observations, *Atmospheric Chemistry
921 and Physics*, 22, 395–418, <https://doi.org/10.5194/acp-22-395-2022>, 2022.

922 Lu, X., Jacob, D. J., Zhang, Y., Shen, L., Sulprizio, M. P., Maasackers, J. D., Varon, D. J., Qu, Z., Chen, Z., Hmiel,
923 B., Parker, R. J., Boesch, H., Wang, H., He, C., and Fan, S.: Observation-derived 2010-2019 trends in methane
924 emissions and intensities from US oil and gas fields tied to activity metrics, *Proceedings of the National Academy of
925 Sciences*, 120, e2217900120, <https://doi.org/10.1073/pnas.2217900120>, 2023.

926 Maasackers, J. D., Jacob, D. J., Sulprizio, M. P., Scarpelli, T. R., Nesser, H., Sheng, J., Zhang, Y., Lu, X., Bloom, A.
927 A., Bowman, K. W., Worden, J. R., and Parker, R. J.: 2010–2015 North American methane emissions, sectoral
928 contributions, and trends: a high-resolution inversion of GOSAT observations of atmospheric methane, *Atmospheric
929 Chemistry and Physics*, 21, 4339–4356, <https://doi.org/10.5194/acp-21-4339-2021>, 2021.

930 Miller, S. M., Wofsy, S. C., Michalak, A. M., Kort, E. A., Andrews, A. E., Biraud, S. C., Dlugokencky, E. J.,
931 Eluskiewicz, J., Fischer, M. L., Janssens-Maenhout, G., Miller, B. R., Miller, J. B., Montzka, S. A., Nehrkorn, T.,
932 and Sweeney, C.: Anthropogenic emissions of methane in the United States, *Proceedings of the National Academy of
933 Sciences*, 110, 20018–20022, <https://doi.org/10.1073/pnas.1314392110>, 2013.

934 Mitchell, A. L., Tkacik, D. S., Roscioli, J. R., Herndon, S. C., Yacovitch, T. I., Martinez, D. M., Vaughn, T. L.,
935 Williams, L. L., Sullivan, M. R., Floerchinger, C., Omara, M., Subramanian, R., Zimmerle, D., Marchese, A. J., and
936 Robinson, A. L.: Measurements of Methane Emissions from Natural Gas Gathering Facilities and Processing Plants:
937 Measurement Results, *Environ. Sci. Technol.*, 49, 3219–3227, <https://doi.org/10.1021/es5052809>, 2015.

938 Nesser, H., Jacob, D. J., Maasackers, J. D., Lorente, A., Chen, Z., Lu, X., Shen, L., Qu, Z., Sulprizio, M. P., Winter,
939 M., Ma, S., Bloom, A. A., Worden, J. R., Stavins, R. N., and Randles, C. A.: High-resolution U.S. methane emissions
940 inferred from an inversion of 2019 TROPOMI satellite data: contributions from individual states, urban areas, and
941 landfills, *EGUsphere*, 1–36, <https://doi.org/10.5194/egusphere-2023-946>, 2023.

942 Ocko, I. B., Sun, T., Shindell, D., Oppenheimer, M., Hristov, A. N., Pacala, S. W., Mauzerall, D. L., Xu, Y., and
943 Hamburg, S. P.: Acting rapidly to deploy readily available methane mitigation measures by sector can immediately
944 slow global warming, *Environ. Res. Lett.*, 16, 054042, <https://doi.org/10.1088/1748-9326/abf9c8>, 2021.

945 Omara, M., Sullivan, M. R., Li, X., Subramanian, R., Robinson, A. L., and Presto, A. A.: Methane Emissions from
946 Conventional and Unconventional Natural Gas Production Sites in the Marcellus Shale Basin, *Environ. Sci. Technol.*,
947 50, 2099–2107, <https://doi.org/10.1021/acs.est.5b05503>, 2016.

948 Omara, M., Zimmerman, N., Sullivan, M. R., Li, X., Ellis, A., Cesa, R., Subramanian, R., Presto, A. A., and Robinson,
949 A. L.: Methane Emissions from Natural Gas Production Sites in the United States: Data Synthesis and National
950 Estimate, *Environ. Sci. Technol.*, 52, 12915–12925, <https://doi.org/10.1021/acs.est.8b03535>, 2018.

951 Omara, M., Zavala-Araiza, D., Lyon, D. R., Hmiel, B., Roberts, K. A., and Hamburg, S. P.: Methane emissions from
952 US low production oil and natural gas well sites, *Nat Commun*, 13, 2085, [https://doi.org/10.1038/s41467-022-29709-](https://doi.org/10.1038/s41467-022-29709-3)
953 3, 2022.

954 Omara, M., Himmelberger, A., MacKay, K., Williams, J. P., Benmergui, J., Sargent, M., Wofsy, S. C., and Gautam,
955 R.: Constructing a measurement-based spatially explicit inventory of US oil and gas methane emissions, *Earth System*
956 *Science Data Discussions*, 1–25, <https://doi.org/10.5194/essd-2024-72>, 2024.

957 Plant, G., Kort, E. A., Brandt, A. R., Chen, Y., Fordice, G., Gorchov Negron, A. M., Schwietzke, S., Smith, M., and
958 Zavala-Araiza, D.: Inefficient and unlit natural gas flares both emit large quantities of methane, *Science*, 377, 1566–
959 1571, <https://doi.org/10.1126/science.abq0385>, 2022.

960 Ravikumar, A. P., Wang, J., McGuire, M., Bell, C. S., Zimmerle, D., and Brandt, A. R.: “Good versus Good Enough?”
961 Empirical Tests of Methane Leak Detection Sensitivity of a Commercial Infrared Camera, *Environ. Sci. Technol.*, 52,
962 2368–2374, <https://doi.org/10.1021/acs.est.7b04945>, 2018.

963 Rella, C. W., Hoffnagle, J., He, Y., and Tajima, S.: Local- and regional-scale measurements of CH₄, δ¹³CH₄, and C₂H₆
964 in the Uintah Basin using a mobile stable isotope analyzer, *Atmospheric Measurement Techniques*, 8, 4539–4559,
965 <https://doi.org/10.5194/amt-8-4539-2015>, 2015.

966 Riddick, S. N., Mauzerall, D. L., Celia, M. A., Kang, M., Bressler, K., Chu, C., and Gum, C. D.: Measuring methane
967 emissions from abandoned and active oil and gas wells in West Virginia, *Science of The Total Environment*, 651,
968 1849–1856, <https://doi.org/10.1016/j.scitotenv.2018.10.082>, 2019.

969 Riddick, S. N., Ancona, R., Mbua, M., Bell, C. S., Duggan, A., Vaughn, T. L., Bennett, K., and Zimmerle, D. J.: A
970 quantitative comparison of methods used to measure smaller methane emissions typically observed from
971 superannuated oil and gas infrastructure, *Atmospheric Measurement Techniques*, 15, 6285–6296,
972 <https://doi.org/10.5194/amt-15-6285-2022>, 2022.

973 Riddick, S. N., Mbua, M., Santos, A., Emerson, E. W., Cheptonui, F., Houlihan, C., Hodshire, A. L., Anand, A.,
974 Hartzell, W., and Zimmerle, D. J.: Methane emissions from abandoned oil and gas wells in Colorado, *Science of The*
975 *Total Environment*, 922, 170990, <https://doi.org/10.1016/j.scitotenv.2024.170990>, 2024.

976 Robertson, A. M., Edie, R., Snare, D., Soltis, J., Field, R. A., Burkhart, M. D., Bell, C. S., Zimmerle, D., and Murphy,
977 S. M.: Variation in Methane Emission Rates from Well Pads in Four Oil and Gas Basins with Contrasting Production
978 Volumes and Compositions, *Environ. Sci. Technol.*, 51, 8832–8840, <https://doi.org/10.1021/acs.est.7b00571>, 2017.

979 Robertson, A. M., Edie, R., Field, R. A., Lyon, D., McVay, R., Omara, M., Zavala-Araiza, D., and Murphy, S. M.:
980 New Mexico Permian Basin Measured Well Pad Methane Emissions Are a Factor of 5–9 Times Higher Than U.S.
981 EPA Estimates, *Environ. Sci. Technol.*, 54, 13926–13934, <https://doi.org/10.1021/acs.est.0c02927>, 2020.

982 Rutherford, J. S., Sherwin, E. D., Ravikumar, A. P., Heath, G. A., Englander, J., Cooley, D., Lyon, D., Omara, M.,
983 Langfitt, Q., and Brandt, A. R.: Closing the methane gap in US oil and natural gas production emissions inventories,
984 *Nat Commun.* 12, 4715, <https://doi.org/10.1038/s41467-021-25017-4>, 2021.

985 Shen, L., Gautam, R., Omara, M., Zavala-Araiza, D., Maasackers, J. D., Scarpelli, T. R., Lorente, A., Lyon, D., Sheng,
986 J., Varon, D. J., Nesser, H., Qu, Z., Lu, X., Sulprizio, M. P., Hamburg, S. P., and Jacob, D. J.: Satellite quantification
987 of oil and natural gas methane emissions in the US and Canada including contributions from individual basins,
988 *Atmospheric Chemistry and Physics*, 22, 11203–11215, <https://doi.org/10.5194/acp-22-11203-2022>, 2022.

989 Sherwin, E., Zhang, Z., Chen, Y., Wetherley, E. B., Yakovlev, P., Berman, E. S. F., Jones, B. B., Thorpe, A. K.,
990 Ayasse, A. K., Duren, R., Brandt, A. R., and Cusworth, D. H.: Quantifying oil and natural gas system emissions using
991 one million aerial site measurements, <https://doi.org/10.21203/rs.3.rs-2406848/v1>, 2023a.

992 Sherwin, E. D., Rutherford, J. S., Chen, Y., Aminfar, S., Kort, E. A., Jackson, R. B., and Brandt, A. R.: Single-blind
993 validation of space-based point-source detection and quantification of onshore methane emissions, *Sci Rep.* 13, 3836,
994 <https://doi.org/10.1038/s41598-023-30761-2>, 2023b.

995 Sherwin, E. D., Rutherford, J. S., Zhang, Z., Chen, Y., Wetherley, E. B., Yakovlev, P. V., Berman, E. S. F., Jones, B.
996 B., Cusworth, D. H., Thorpe, A. K., Ayasse, A. K., Duren, R. M., and Brandt, A. R.: US oil and gas system emissions
997 from nearly one million aerial site measurements, *Nature*, 627, 328–334, [https://doi.org/10.1038/s41586-024-07117-](https://doi.org/10.1038/s41586-024-07117-5)
998 5, 2024.

999 Stavropoulou, F., Vinković, K., Kers, B., de Vries, M., van Heuven, S., Korbeň, P., Schmidt, M., Wietzel, J., Jagoda,
1000 P., Necki, J. M., Bartyzel, J., Maazallahi, H., Menoud, M., van der Veen, C., Walter, S., Tuzson, B., Ravelid, J.,
1001 Morales, R. P., Emmenegger, L., Brunner, D., Steiner, M., Hensen, A., Velzeboer, I., van den Bulk, P., Denier van
1002 der Gon, H., Delre, A., Edjabou, M. E., Scheutz, C., Corbu, M., Iancu, S., Moaca, D., Scarlat, A., Tudor, A., Vizireanu,
1003 I., Calcan, A., Ardelean, M., Ghemulet, S., Pana, A., Constantinescu, A., Cusa, L., Nica, A., Baciu, C., Pop, C.,
1004 Radovici, A., Mereuta, A., Stefanie, H., Dandocsi, A., Hermans, B., Schwietzke, S., Zavala-Araiza, D., Chen, H., and
1005 Röckmann, T.: High potential for CH₄ emission mitigation from oil infrastructure in one of EU’s major production
1006 regions, *Atmospheric Chemistry and Physics*, 23, 10399–10412, <https://doi.org/10.5194/acp-23-10399-2023>, 2023.

1007 Thorpe, M. J., Krietinger, A., Altamura, D., Dudiak, C. D., Conrad, B. M., Tyner, D. R., Johnson, M. R., Brasseur, J.
1008 K., Roos, P., Kunkel, W., Carre-Burritt, A., Abate, J., Price, T., Yaralian, D., Kennedy, B., Newton, E., Rodriguez,
1009 E., Elfar, O. I., and Zimmerle, D. J.: Deployment-invariant probability of detection characterization for aerial LiDAR
1010 methane detection, 2024.

1011 Tyner, D. R. and Johnson, M. R.: Where the Methane Is—Insights from Novel Airborne LiDAR Measurements
1012 Combined with Ground Survey Data, *Environ. Sci. Technol.*, 55, 9773–9783, <https://doi.org/10.1021/acs.est.1c01572>,
1013 2021.

1014 Inventory of U.S. Greenhouse Gas Emissions and Sinks: [https://www.epa.gov/ghgemissions/inventory-us-](https://www.epa.gov/ghgemissions/inventory-us-greenhouse-gas-emissions-and-sinks)
1015 [greenhouse-gas-emissions-and-sinks](https://www.epa.gov/ghgemissions/inventory-us-greenhouse-gas-emissions-and-sinks), last access: 6 March 2024.

1016 EPA’s Final Rule for Oil and Natural Gas Operations Will Sharply Reduce Methane and Other Harmful Pollution.:
1017 <https://www.epa.gov/controlling-air-pollution-oil-and-natural-gas-operations/epas-final-rule-oil-and-natural-gas>, last
1018 access: 5 March 2024.

1019 Weller, Z. D., Hamburg, S. P., and von Fischer, J. C.: A National Estimate of Methane Leakage from Pipeline Mains
1020 in Natural Gas Local Distribution Systems, *Environ. Sci. Technol.*, 54, 8958–8967,
1021 <https://doi.org/10.1021/acs.est.0c00437>, 2020.

1022 Williams, J. P., Regehr, A., and Kang, M.: Methane Emissions from Abandoned Oil and Gas Wells in Canada and the
1023 United States, *Environ. Sci. Technol.*, 55, 563–570, <https://doi.org/10.1021/acs.est.0c04265>, 2021.

1024 Williams, J. P., El Hachem, K., and Kang, M.: Controlled-release testing of the static chamber methodology for direct
1025 measurements of methane emissions, *Atmospheric Measurement Techniques*, 16, 3421–3435,
1026 <https://doi.org/10.5194/amt-16-3421-2023>, 2023.

1027 Worden, J. R., Cusworth, D. H., Qu, Z., Yin, Y., Zhang, Y., Bloom, A. A., Ma, S., Byrne, B. K., Scarpelli, T.,
1028 Maasackers, J. D., Crisp, D., Duren, R., and Jacob, D. J.: The 2019 methane budget and uncertainties at 1° resolution
1029 and each country through Bayesian integration Of GOSAT total column methane data and a priori inventory estimates,
1030 *Atmospheric Chemistry and Physics*, 22, 6811–6841, <https://doi.org/10.5194/acp-22-6811-2022>, 2022.

1031 Xia, H., Strayer, A., and Ravikumar, A. P.: The Role of Emission Size Distribution on the Efficacy of New
1032 Technologies to Reduce Methane Emissions from the Oil and Gas Sector, *Environ. Sci. Technol.*, 58, 1088–1096,
1033 <https://doi.org/10.1021/acs.est.3c05245>, 2024.

1034 Yacovitch, T. I., Herndon, S. C., Pétron, G., Kofler, J., Lyon, D., Zahniser, M. S., and Kolb, C. E.: Mobile Laboratory
1035 Observations of Methane Emissions in the Barnett Shale Region, *Environ. Sci. Technol.*, 49, 7889–7895,
1036 <https://doi.org/10.1021/es506352j>, 2015.

1037 Zhang, Y., Gautam, R., Pandey, S., Omara, M., Maasackers, J. D., Sadavarte, P., Lyon, D., Nesser, H., Sulprizio, M.
1038 P., Varon, D. J., Zhang, R., Houweling, S., Zavala-Araiza, D., Alvarez, R. A., Lorente, A., Hamburg, S. P., Aben, I.,
1039 and Jacob, D. J.: Quantifying methane emissions from the largest oil-producing basin in the United States from space,
1040 *Science Advances*, 6, eaaz5120, <https://doi.org/10.1126/sciadv.aaz5120>, 2020.

1041 Zhou, X., Yoon, S., Mara, S., Falk, M., Kuwayama, T., Tran, T., Cheadle, L., Nyarady, J., Croes, B., Scheehle, E.,
1042 Herner, J. D., and Vijayan, A.: Mobile sampling of methane emissions from natural gas well pads in California,
1043 *Atmospheric Environment*, 244, 117930, <https://doi.org/10.1016/j.atmosenv.2020.117930>, 2021.

1044 Zimmerle, D., Vaughn, T., Luck, B., Lauderdale, T., Keen, K., Harrison, M., Marchese, A., Williams, L., and Allen,
1045 D.: Methane Emissions from Gathering Compressor Stations in the U.S., *Environ. Sci. Technol.*, 54, 7552–7561,
1046 <https://doi.org/10.1021/acs.est.0c00516>, 2020.

1047

1048

1049

1050

1051

1052

1053

1054

